Deep-mantle krypton reveals Earth's early accretion of carbonaceous matter

https://doi.org/10.1038/s41586-021-04092-z

Received: 29 September 2020

Accepted: 4 October 2021

Published online: 15 December 2021

Check for updates

Sandrine Péron[1]✉, Sujoy Mukhopadhyay[1], Mark D. Kurz[2] & David W. Graham[3]

Establishing when, and from where, carbon, nitrogen and water were delivered to Earth is a fundamental objective in understanding the origin of habitable planets such as Earth. Yet, volatile delivery to Earth remains controversial[1–5]. Krypton isotopes provide insights on volatile delivery owing to their substantial isotopic variations among sources[6–10], although pervasive atmospheric contamination has hampered analytical efforts. Here we present the full suite of krypton isotopes from the deep mantle of the Galápagos and Iceland plumes, which have the most primitive helium, neon and tungsten isotopic compositions[11–16]. Except for ^{86}Kr, the krypton isotopic compositions are similar to a mixture of chondritic and atmospheric krypton. These results suggest early accretion of carbonaceous material by proto-Earth and rule out any combination of hydrodynamic loss with outgassing of the deep or shallow mantle to explain atmospheric noble gases. Unexpectedly, the deep-mantle sources have a deficit in the neutron-rich ^{86}Kr relative to the average composition of carbonaceous meteorites, which suggests a nucleosynthetic anomaly. Although the relative depletion of neutron-rich isotopes on Earth compared with carbonaceous meteorites has been documented for a range of refractory elements[1,17,18], our observations suggest such a depletion for a volatile element. This finding indicates that accretion of volatile and refractory elements occurred simultaneously, with krypton recording concomitant accretion of non-solar volatiles from more than one type of material, possibly including outer Solar System planetesimals.

Volatile delivery was a key process that shaped Earth's early surface environment. Yet the timing and sources of volatile delivery, as well as subsequent volatile evolution, are still debated[1–5,19]. Although some studies advocate for most volatile delivery before the last giant impact[5,19], a contribution from a late veneer event may also be required[1,2]. Three main sources seem to be needed to explain the Earth's volatile composition, namely solar[3,4,20], chondritic[20] and cometary[21]. The study of accretional heterogeneities preserved in the deep mantle provides direct observational constraints for testing planet-formation models, in particular regarding the processes responsible for material migration in the Solar System[1,3]. For instance, dual accretion of volatile-rich outer Solar System material and solar gases in the deep Earth[10,22] may indicate early transport of outer Solar System solids into Earth's formation region[23].

Being inert, noble gases are ideal tracers of volatile sources and evolution[3,4]. However, Earth's deep-mantle noble gas composition remains poorly constrained, particularly for krypton (Kr) and xenon (Xe). Krypton, with its six stable isotopes—^{78}Kr, ^{80}Kr, ^{82}Kr, ^{83}Kr, ^{84}Kr and ^{86}Kr—is extremely well suited to deconvolve solar from chondritic sources because they have distinct isotopic compositions; solar and chondritic material are enriched in light and heavy Kr isotopes relative to Earth's atmosphere, respectively[24,25]. Upper-mantle Kr appears chondritic rather than solar on the basis of measured ^{82}Kr/^{84}Kr and ^{86}Kr/^{84}Kr ratios in carbon dioxide (CO_2) well gases[9]. Measurement of the ^{86}Kr/^{84}Kr ratio from a single mid-ocean-ridge basalt (MORB) is also consistent with chondritic Kr in the upper mantle[8]. A recent investigation of deep-mantle Kr and Xe isotopes in volcanic gases from the Yellowstone hotspot suggests a chondritic origin[10]. As neon (Ne) isotopes in basalts derived from the deep mantle indicate acquisition of a solar component during the early phase of Earth's accretion[4,26,27], the Yellowstone results could indicate a dual solar and chondritic source during early terrestrial accretion[10]. The fingerprint of crustal and lithospheric mantle helium (He) and Ne in the Yellowstone gas samples[10], however, leaves room for the possibility that Kr in these samples may be derived from a source less primitive than other hotspots such as Hawaii, Iceland and Galápagos. In addition, the mantle compositions of the light isotopes ^{78}Kr and ^{80}Kr are not known owing to their very low abundances, ubiquitous atmospheric contamination and progressive atmospheric noble gas recycling into the mantle. As we show, these isotopes are critical for determining the volatile sources for Kr, and by inference Xe.

Deep-mantle Kr and Xe

We analysed the Kr isotopic composition of ocean island basalt (OIB) glass samples from Fernandina, Galápagos and from Midfell, Iceland. These two hotspots sample the deep mantle via plumes rooted at the core–mantle boundary[28] and the samples analysed have the most

[1]Department of Earth and Planetary Sciences, University of California, Davis, Davis, CA, USA. [2]Marine Chemistry and Geochemistry, Woods Hole Oceanographic Institution, Woods Hole, MA, USA. [3]College of Earth, Ocean, and Atmospheric Sciences, Oregon State University, Corvallis, OR, USA. ✉e-mail: scperon@ucdavis.edu

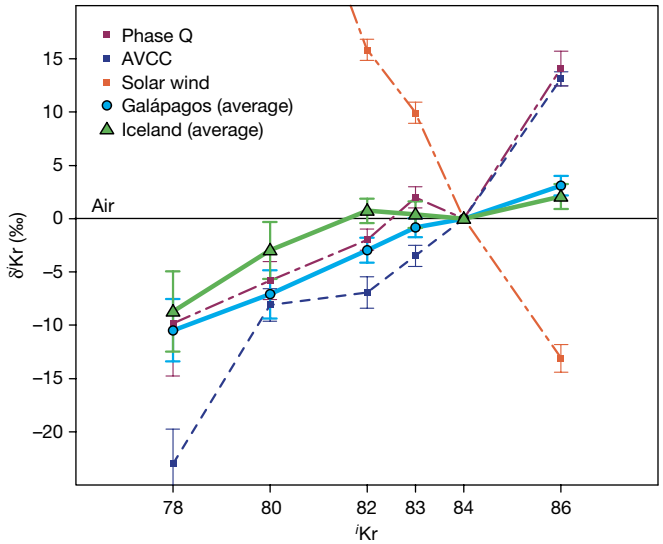

Fig. 1 | Krypton isotopic patterns of Galápagos and Iceland samples. Isotopic ratios are in delta notation, $\delta^{i}\mathrm{Kr} = ((^{i}\mathrm{Kr}/^{84}\mathrm{Kr})_{\mathrm{sample}}/(^{i}\mathrm{Kr}/^{84}\mathrm{Kr})_{\mathrm{air}} - 1) \times 10^{3}$. The average Kr isotopic compositions of the four Galápagos (solid blue line) and the two Iceland (solid green line) measurements are compared with Phase Q (dashed purple line)[25], AVCC (dashed dark blue line) and solar wind (dashed orange line)[24]. The δ^{78}Kr and δ^{80}Kr of solar wind are 54.2‰ and 40.4‰, respectively. The measured Kr isotopic ratios in the Galápagos and Iceland plume sources are close to Phase Q[25]; compared with δ^{78}Kr and δ^{80}Kr of −9.9 ± 4.9‰ and −5.8 ± 1.8‰, respectively, for Phase Q[25], the Galápagos values are −10.5 ± 2.9‰ and −7.1 ± 2.3‰, respectively. For Iceland, δ^{78}Kr and δ^{80}Kr are −8.7 ± 3.8‰ and −3.0 ± 2.7‰, respectively. The error bars are 1σ.

primitive Ne compositions[11,13–16]. Furthermore, both plumes have negative tungsten (W) isotope anomalies, with Galápagos carrying the largest negative anomaly[12]. To overcome the challenges of low noble gas abundances and ubiquitous shallow-level atmospheric contamination in basalts[29], we used the novel technique of accumulating argon (Ar), Kr and Xe from crushing steps that show little atmospheric contamination as determined by analyses of Ne isotopes[8], followed by an effective Ar–Kr–Xe separation and multicollection of five Kr isotopes during the mass spectrometric analyses (Methods).

The Kr isotopic compositions of Galápagos and Iceland (Extended Data Table 1) are distinct from air and solar wind but similar to the chondritic end-member (Fig. 1, Extended Data Figs. 1, 2). The measured ^{82}Kr/^{84}Kr and ^{86}Kr/^{84}Kr ratios of both plumes are similar to the highest measured values of the upper mantle based on CO_2 well gases[9] and one MORB sample[8] (Fig. 2). Whether this similarity extends to the lighter isotope ratios ^{78}Kr/^{84}Kr and ^{80}Kr/^{84}Kr remains to be determined because these ratios have not been established for the upper mantle. The Galápagos and Iceland Kr ratios are similar to one sample from the Yellowstone hotspot[10] but differ from a second sample (Fig. 2), the reasons for which are not entirely clear.

The Xe isotopic data of Galápagos and Iceland are reported in Extended Data Table 2 and shown in Fig. 3. Although there are no literature data for Galápagos, the new Iceland data are in very good agreement with literature data for Xe[14,15]. The Iceland accumulated gas is similar in composition to the error-weighted step-crush average of the DICE sample (Supplemental Fig. 5 of ref. [14]), which provides confidence for the Kr isotope data. However, the error-weighted DICE average[14] is closer to air because of a greater atmospheric contamination (Fig. 3). The Galápagos accumulated gas is also very similar in composition to the DICE error-weighted step-crush average[14]. Importantly, our Xe data do not plot on a mass fractionation line (Fig. 3). The non-radiogenic ^{124}Xe/^{130}Xe and ^{126}Xe/^{130}Xe ratios are not resolved from air. But the Galápagos and Iceland non-radiogenic ^{128}Xe/^{130}Xe ratios show slight excesses relative to air. In the ^{128}Xe/^{130}Xe–^{129}Xe/^{130}Xe space, the Galápagos average barely overlaps with the best-fit mixing line between the atmosphere and upper-mantle samples[8,30–32], while the Iceland average appears to fall on the line. Whereas the Yellowstone plume data appear to fall on a steeper mixing line than the upper mantle[10], the uncertainty in the Galápagos and Iceland data do not allow us to conclude whether they are on the same mixing line defined by samples from the upper mantle[8,30–32] or a slightly steeper mixing line.

Recycled proportion of atmospheric Kr

The clear observation of non-atmospheric Kr in the Galápagos and Iceland sources provides firm constraints on the amount of atmospheric Kr recycled into the deep mantle through subduction[31,33]. For primordial mantle Kr, we use two meteoritic reference points, average carbonaceous chondrites (AVCC; Methods, Extended Data Table 3) and Phase Q, which is a poorly characterized carbonaceous phase carrying the majority of trapped heavy noble gases in meteorites[25]. Phase Q is widespread in chondrites and usually the only trapped component in achondrites[25,34,35], whereas carbonaceous chondrites are the meteorite group for which there is currently the most precise Kr isotopic data. If the primordial plume-source Kr composition is assumed to be equivalent to AVCC, or to Phase Q, the proportion of atmospheric Kr in the plume source would range from 64 ± 8% to 0^{+9}_{0}% (Fig. 4, Methods). Likewise, we can place upper bounds on the amount of solar Kr in the deep mantle by assuming a solar–AVCC mixture, which constrains the solar component to be 10 ± 2% and 16 ± 2% of the Kr in the Galápagos and Iceland plumes, respectively (Fig. 4).

The measured Kr and Xe isotopic anomalies from Galápagos and Iceland are lower limits of the isotopic anomalies in the mantle sources of these two plumes because the measured values have not been entirely corrected for shallow-level atmospheric contamination; the gas accumulation methodology drastically reduces atmospheric contamination but does not eliminate it[8] (Methods). Thus, the maximum proportions of recycled atmospheric Kr are 48 ± 8% and 64 ± 8% for the Galápagos and Iceland sources, respectively, assuming AVCC as the initial composition (Fig. 4). The proportions of recycled air in the mantle plumes suggest that the Galápagos source may have retained a more primitive heavy noble gas signature than the Iceland source, consistent with the less radiogenic ^{3}He/^{4}He ratios, the less nucleogenic ^{21}Ne/^{22}Ne ratios and the more negative μ^{182}W (deviation of ^{182}W/^{184}W from terrestrial standards in parts per million) in the Galápagos source[11–16]. Using the ^{128}Xe excesses, we estimate the maximum proportion of recycled atmospheric Xe in the deep mantle. Assuming an initial composition similar to AVCC, at maximum, 93 ± 5% and 95^{+5}_{-6}% of the ^{130}Xe budget are of recycled origin for the Galápagos and Iceland mantle sources, respectively. The percentage of recycled ^{130}Xe in the Iceland plume based only on the ^{128}Xe/^{130}Xe ratio from this study is in good agreement with the $93.4^{+2.4}_{-1.2}$% estimated previously for the Iceland plume using ^{130,131,132,134,136}Xe (ref. [33]). As a comparison, for plume-influenced samples from the Rochambeau Rift in the Lau Basin, $88.8^{+3.1}_{-1.2}$% of ^{130}Xe is from recycling[33,36]. Importantly, the maximum proportion of recycled Kr in the plumes is lower than the minimum proportion of recycled Xe, demonstrating that Kr in the mantle is much less affected by recycling than Xe.

Sources of Earth's volatiles

To determine the origin of primordial Kr, we investigate the full suite of Kr isotopes, which indicates that the measured ^{78,80,82,83}Kr/^{84}Kr ratios in both plumes are similar to that of Phase Q[25] (Fig. 1). The Kr isotopic anomalies, relative to air, are slightly lower for the Iceland sample, but within uncertainties of the Galápagos values (Figs. 1, 2).

Despite the similarity of the light Kr isotopes with Phase Q, the initial deep-mantle Kr isotopic composition cannot be derived solely from Q.

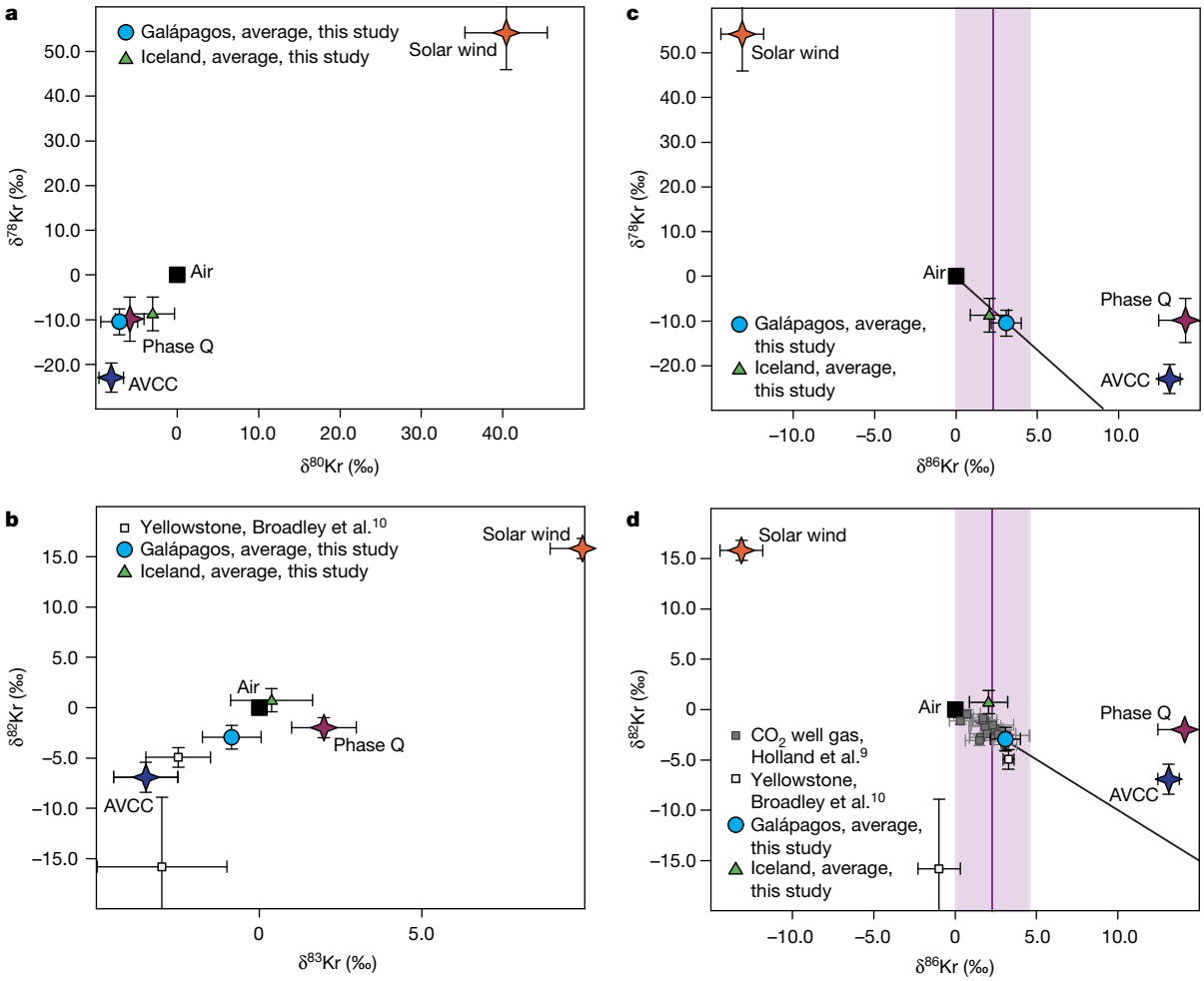

Fig. 2 | Krypton isotopic compositions of Galápagos and Iceland samples. a, δ^{78}Kr versus δ^{80}Kr. **b**, δ^{82}Kr versus δ^{83}Kr. **c**, δ^{78}Kr versus δ^{86}Kr. **d**, δ^{82}Kr versus δ^{86}Kr. The Galápagos and Iceland data are the averages of the four D22 and two DG2017 measurements, respectively. Air, Phase Q[25], AVCC (Extended Data Table 3) and solar wind[24] are shown for comparison. Data for CO_2 well gases (corrected for crustal fission) and Yellowstone are also indicated, but only ^{82}Kr, ^{83}Kr, ^{84}Kr and ^{86}Kr have been measured[9,10]. The solid lines in **c**, **d** highlight the deficit in ^{86}Kr relative to the chondritic end-member. The measured δ^{82}Kr and δ^{86}Kr of the two mantle plumes (δ^{82}Kr of −2.9 ± 1.2‰ and 0.7 ± 1.1‰, δ^{86}Kr of 3.1 ± 0.9‰ and 2.1 ± 1.2‰ for Galápagos and Iceland, respectively) are similar to the highest measured δ^{82}Kr (−0.44 ± 0.46‰) and δ^{86}Kr (3.17 ± 1.44‰) ratios of the upper mantle based on analyses of CO_2 well gases[9] and to the δ^{86}Kr (2.29 ± 2.29‰, purple bar in **c**, **d**) of the Mid-Atlantic Ridge popping rock basalt[8]. Data for the Galápagos and Iceland hotspots rule out any substantial solar contribution for heavy noble gases in the deep mantle. The error bars are 1σ.

The measured δ^{86}Kr (per mil deviation of ^{86}Kr/^{84}Kr from air) for both plumes are much lower than the value for Q. On the basis of the calculated proportions of a Phase Q–air mixture (Fig. 4), the expected δ^{86}Kr are 14.1 ± 1.3‰ for Galápagos and 10.1 ± 2.6‰ for Iceland, much higher than their respective measured values of 3.09 ± 0.92‰ and 2.06 ± 1.17‰ (Fig. 5).

Carbonaceous chondrites may represent a possible source of Kr, and therefore other volatiles, for the deep mantle (Figs. 1, 2). On the basis of the mixing proportions of AVCC–air Kr (Fig. 4), the expected δ^{86}Kr is 6.85 ± 0.98‰ for Galápagos and 4.71 ± 0.98‰ for Iceland, much higher than the measured values (Fig. 5). Given the uncertainties in the measured and predicted values, the probability that the measured δ^{86}Kr values for both the Galápagos and Iceland are lower than the predicted values by random chance is 0.01% (Extended Data Fig. 3); that is, there is a 99.99% probability that Earth's mantle has a deficit in the heaviest Kr isotopes with respect to the average composition of carbonaceous chondrites. Given the small dataset and the limited precision on Kr isotopic ratios for different carbonaceous chondrite groups (Extended Data Table 3), we cannot rule out that a specific group of carbonaceous chondrites may match the Earth's deep-mantle Kr isotopic composition. However, dynamically, several types of carbonaceous chondrite would be expected to be scattered to the inner Solar System during Earth's formation.

The misfit to the deep mantle's δ^{86}Kr would be larger for ordinary and enstatite chondrites (Extended Data Table 3) because they have higher ^{86}Kr/^{84}Kr values than AVCC. Likewise, a mix of solar–AVCC Kr predicts much higher δ^{86}Kr (Fig. 5). Consequently, the deep mantle has a nucleosynthetic ^{86}Kr anomaly with respect to AVCC, enstatite and ordinary chondrites, and solar compositions; the average composition of carbonaceous chondrites though provides the closest match. The nucleosynthetic ^{86}Kr anomaly is more visible in the Galápagos plume given its higher proportion of primordial Kr compared with Iceland (Fig. 4).

The nucleosynthetic ^{86}Kr anomaly of the two hotspots must be a remnant of Earth's accretion, signifying that some planetary building blocks carried a lower ^{86}Kr/^{84}Kr ratio than represented by the AVCC composition or Phase Q. The δ^{86}Kr of slow-process nucleosynthesis, determined through analyses of interstellar silicon carbide (SiC) from the Murchison carbonaceous chondrite, shows a wide range[37] from −223‰ to +3,041‰ (ref. [38]), requiring several stellar sources to have contributed SiC grains to the parent molecular cloud of the Solar System[38]. The large variability in δ^{86}Kr of SiC grains occurs as ^{86}Kr is at a branching point on the slow-process path. Incomplete mixing of SiC grains, derived from asymptotic giant branch (AGB) stars, in the solar nebula might then have imparted varying ^{86}Kr/^{84}Kr ratios in different parent bodies with

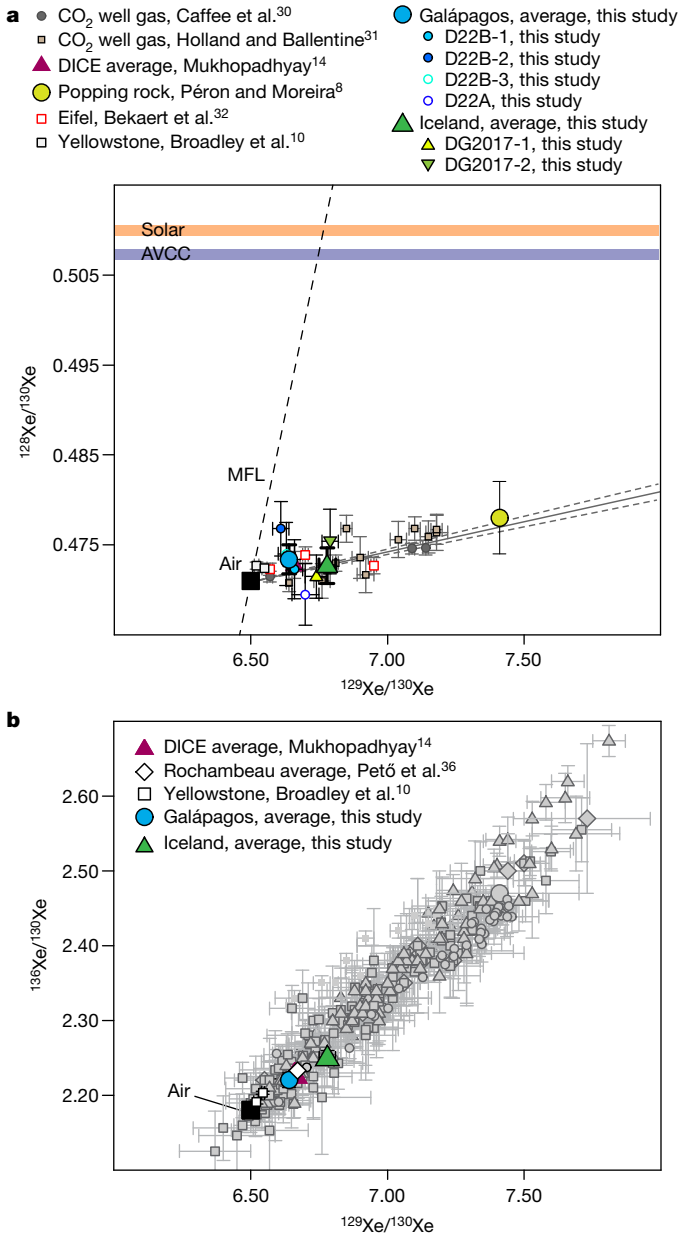

Fig. 3 | Xenon isotope composition of Galápagos and Iceland samples. a, $^{128}Xe/^{130}Xe$–$^{129}Xe/^{130}Xe$. The Galápagos and Iceland data are the averages of the four D22 (small circles) and two DG2017 (small triangles) measurements, respectively. Literature data for upper-mantle-derived samples from CO_2 well gases[30,31], the Mid-Atlantic Ridge popping rock basalt[8], thermal springs from Eifel[32] and plume source samples from Iceland (error-weighted average of all crush steps of DICE)[14] and from Yellowstone[10] are shown for comparison. The data for Eifel[32] and Yellowstone[10] are normalized to the same atmospheric composition used in this study (Extended Data Table 2). MFL stands for mass fractionation line (dashed line). Our data for Galápagos and Iceland (averages and individual data points) are not on the MFL. The solid and dashed grey lines represent the mixing line (error-weighted fit forced through air) defined by upper-mantle-derived samples with the 68% confidence interval. **b**, $^{136}Xe/^{130}Xe$–$^{129}Xe/^{130}Xe$. The plume samples (this study, DICE error-weighted average[14], Rochambeau error-weighted average[36] and Yellowstone[10]) compared with upper-mantle samples (refer to Methods for references). The error bars on measurements are 1σ.

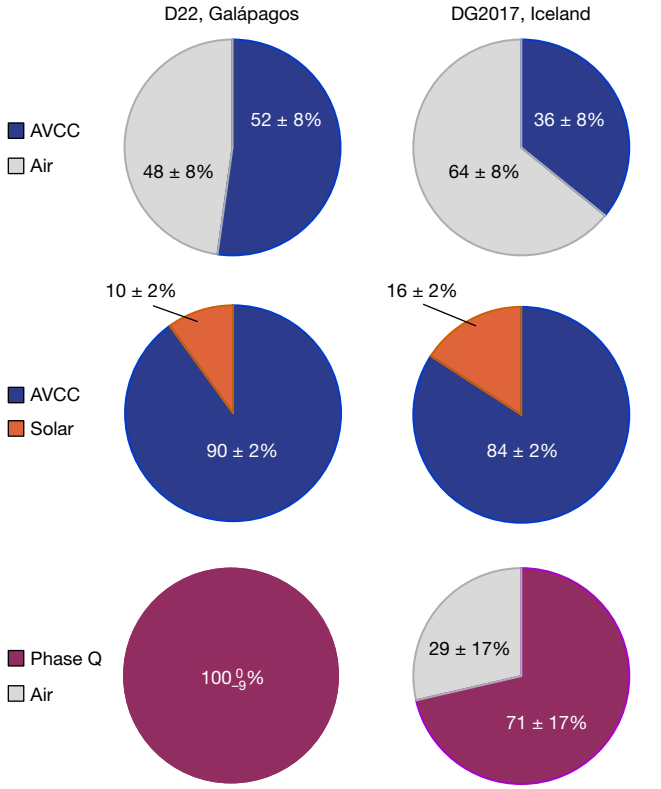

Fig. 4 | Mixing proportions in the plume sources. Estimates of mixing proportions to explain the ^{78}Kr–^{80}Kr–^{84}Kr compositions of samples D22A and D22B (Galápagos) and DG2017 (Iceland). Three scenarios have been considered: mixing of AVCC with air, mixing of AVCC with a solar end-member and mixing of Phase Q with air. The error bars are 1σ.

some carrying ^{86}Kr depletion relative to the average composition of carbonaceous chondrites. However, we cannot rule out the possibility that rapid-process nucleosynthesis associated with supernovae may also have produced variability in the neutron-rich Kr isotopic ratio as ^{86}Kr is not shielded from rapid-process nucleosynthesis.

Several refractory elements (for example, calcium (Ca), titanium (Ti), chromium (Cr), nickel (Ni), zirconium (Zr), molybdenum (Mo), ruthenium (Ru) and neodymium (Nd)) on Earth show relative depletions in neutron-rich isotopes in reference to carbonaceous meteorites[1,17,18]. These depletions have been attributed to a relative enrichment of slow-process over rapid-process matter, as well as to heterogeneous distribution of grains derived from different AGB stars in Earth-forming materials[1,17,18]. Isotopes of refractory elements such as Ca and Ti track the composition of accreted material throughout Earth's formation[17,39]. Hence, the observed relative depletion in a neutron-rich isotope for the highly volatile element Kr in the solid Earth (Fig. 5) suggests that its depletion may be linked to relative depletion of the neutron-rich refractory elements on Earth, indicating that accretion of volatile and refractory elements occurred simultaneously.

Earth's deep mantle deficit in ^{86}Kr has ramifications for the longstanding debate about the origin of terrestrial Xe, as the heavy noble gases (Kr and Xe) are thought to have a common origin on Earth[9,10]. The initial Xe in Earth's mantle and atmosphere was long advocated to be U-Xe[40], a primordial component with a deficit in the neutron-rich isotopes ^{134}Xe and ^{136}Xe (ref. [41]), but never directly observed in a parent body. Recently, U-Xe was shown to be a mixture of chondritic and cometary Xe[21], establishing an observational basis for Earth's initial atmospheric composition. However, for the mantle, chondritic Xe, and not U-Xe, has been suggested as the progenitor[8–10], although differences between chondritic and U-Xe are not discernible given the measurement uncertainties. Instead, the Kr isotopic results suggest that Earth's mantle may well have a deficit of the neutron-rich Xe isotopes with respect to chondrites; that is, a U-Xe pattern reflecting a mixture of chondritic and cometary Xe[21].

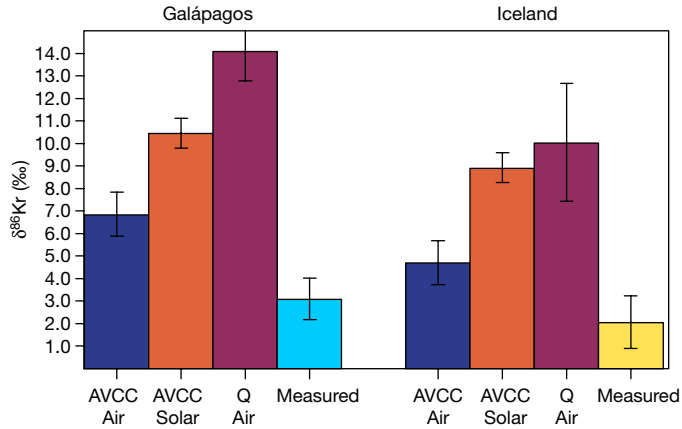

Fig. 5 | Estimated ^{86}Kr/^{84}Kr ratio based on different mixing scenarios. Predicted ^{86}Kr/^{84}Kr ratio (expressed in delta unit, per mil deviation relative to the air ratio) based on the calculated mixing proportions (Fig. 4) for samples D22 from Galápagos (left) and DG2017 from Iceland (right). These predicted ratios are compared with the average measured ratios for each sample. The comparison shows that the measured ^{86}Kr/^{84}Kr ratios are lower than expected based on the measured ^{78}Kr and ^{80}Kr anomalies. The error bars are σ.

To further evaluate the possible sources of deep mantle Kr, we investigate the nature of the accretionary material. Earth may have primarily grown from differentiated planetesimals as sampled in achondrites[42]. In differentiated meteorites, Kr is mainly hosted in Phase Q[25,34]. However, it is unlikely that deep-mantle Kr is only from Phase Q (Figs. 4, 5). If Earth grew from differentiated planetesimals, then either the achondrite parent bodies had much lower ^{86}Kr/^{84}Kr ratios than Phase Q owing to the presence of other nucleosynthetic components, unlike those that have been observed[25,34,35], or additional parent bodies with a low ^{86}Kr/^{84}Kr ratio were also added. The nature of the ^{86}Kr-depleted parent body is not entirely clear. The only planetary body that has so far been shown to carry a deficit in ^{86}Kr relative to solar wind is the Kuiper Belt comet 67P/Churyumov–Gerasimenko[43]. Accretion of cometary material would also have produced a depletion in the heavy Xe isotopes[21], leading to a U-Xe composition of the deep mantle. Owing to the large uncertainty in the cometary Kr composition[43] a mixing calculation to determine the proportion of cometary Kr required to explain the deep-mantle Kr isotopic composition is not feasible.

The measured Kr isotopic composition may be explained by accretion of a specific group of carbonaceous chondrites, or parent bodies carrying noble gases in the carbonaceous Phase Q, such as enstatite or ordinary chondrites[25], with other parent bodies, potentially comets, carrying a depletion in the neutron-rich ^{86}Kr isotope. The enstatite or ordinary chondrite parent bodies would require a larger contribution from a parent body depleted in ^{86}Kr. However, as Phase Q is carbonaceous and widespread in chondrites and achondrites[25,34], all scenarios require early accretion of carbonaceous phases. The discussions above highlight that one or more volatile-rich outer Solar System objects probably contributed to the deep mantle's Kr budget during the earliest phase of Earth's accretion.

Implications for origin of atmosphere

The primordial Kr sampled by the mantle plumes had to be delivered during the early phases of Earth accretion. Indeed, mantle plumes sample a reservoir that differentiated from the upper mantle before the end of Earth's main phase of accretion (that is, by 4.45 billion years ago) and has never been homogenized with the rest of the mantle based on its μ^{182}W, iodine/plutonium (I/Pu)-derived Xe, and ^{3}He/^{22}Ne ratios[14,33,36]. Early Kr delivery associated with carbonaceous phases, or chondritic parent bodies, also suggests simultaneous delivery of other chondritic volatiles. This early delivery was concurrent with acquisition of solar Ne in the deep mantle[10,22]. As the solar wind and solar nebula are enriched by several orders of magnitude in Ne relative to Kr and because the solar Ne/Kr ratio is also several orders of magnitude higher than in chondrites, acquisition of solar Ne would not affect the Kr composition[10,44,45]. We propose that the composition of volatile elements suggests that delivery was not restricted towards the end of the accretion, or to the aftermath of the Moon-forming giant impact. Rather, volatile delivery may have occurred through most of Earth's accretion with volatile abundances on the growing planet sculpted and fractionated by processes such as core formation and atmospheric loss.

Volatile delivery during only the early or the main phase of Earth's accretion, however, does not explain the atmospheric noble gases—the largest reservoir of noble gases on Earth. Degassing of chondritic Kr from the upper mantle does not match the atmospheric composition (Fig. 2). As hydrodynamic escape would leave a residual atmosphere enriched in the heavier isotopes, degassing of the upper mantle followed by hydrodynamic escape also cannot explain the atmospheric composition[9]. Similarly, the deep-mantle enrichment in heavy Kr isotopes compared with the atmosphere (Figs. 1, 2) indicates that any combination of deep and shallow mantle outgassing followed by hydrodynamic escape will not produce the atmospheric composition. The chemical similarity between Earth and the Moon is used to argue for isotopic equilibration between Earth's mantle and the impacting body, either through a silicate vapour disk[46] or through a synestia-like planetary structure generated by vaporizing a portion of the silicate Earth through high-angular-momentum impacts[47]. If isotopic equilibration of refractory lithophile isotopes between Earth's silicate mantle and the impactor was achieved, the pre-existing atmosphere on Earth should also have equilibrated with its silicate interior. Hence, we hypothesize that a large fraction of atmospheric noble gases was delivered after the last major equilibration of the mantle with the atmosphere—the Moon-forming giant impact[46,47]. Consequently, volatile delivery during the late veneer is also required to explain the atmospheric noble gases[9,48].

The recognition of the deep mantle's Kr isotopic patterns suggests an outer Solar System contribution to Earth's volatile budget starting early in Earth's accretion history. Carbonaceous or organic-rich material could have been delivered to the inner Solar System during radial transport of dust-sized grains in the disk before the formation of Jupiter[49]. In addition, during giant planet formation and migration in the nebula, volatile-rich planetesimals from the outer Solar System could have been scattered onto terrestrial planet-crossing orbits[23,50]. In either scenario, volatile-rich material from the outer Solar System was delivered into the terrestrial planet-forming region during the early periods of Earth's accretion.

Online content

Any methods, additional references, Nature Research reporting summaries, source data, extended data, supplementary information, acknowledgements, peer review information; details of author contributions and competing interests; and statements of data and code availability are available at https://doi.org/10.1038/s41586-021-04092-z.

1. Fischer-Gödde, M. et al. Ruthenium isotope vestige of Earth's pre-late-veneer mantle preserved in Archaean rocks. *Nature* **579**, 240–244 (2020).
2. Albarède, F. Volatile accretion history of the terrestrial planets and dynamic implications. *Nature* **461**, 1227–1233 (2009).
3. Mukhopadhyay, S. & Parai, R. Noble gases: a record of Earth's evolution and mantle dynamics. *Annu. Rev. Earth Planet. Sci.* **47**, 389–419 (2019).
4. Moreira, M. Noble gas constraints on the origin and evolution of Earth's volatiles. *Geochem. Perspect.* **2**, 229–403 (2013).
5. Clay, P. L. et al. Halogens in chondritic meteorites and terrestrial accretion. *Nature* **551**, 614–618 (2017).

6. Ozima, M. & Zashu, S. Solar-type Ne in Zaire cubic diamonds. *Geochim. Cosmochim. Acta* **52**, 19–25 (1988).
7. Ozima, M. & Zashu, S. Noble gas state of the ancient mantle as deduced from noble gases in coated diamonds. *Earth Planet. Sci. Lett.* **105**, 13–27 (1991).
8. Péron, S. & Moreira, M. Onset of volatile recycling into the mantle determined by xenon anomalies. *Geochem. Perspect. Lett.* **9**, 21–25 (2018).
9. Holland, G., Cassidy, M. & Ballentine, C. J. Meteorite Kr in Earth's mantle suggests a late accretionary source for the atmosphere. *Science* **326**, 1522–1525 (2009).
10. Broadley, M. W. et al. Identification of chondritic krypton and xenon in Yellowstone gases and the timing of terrestrial volatile accretion. *Proc. Natl Acad. Sci. USA* **117**, 13997–14004 (2020).
11. Péron, S. et al. Neon isotopic composition of the mantle constrained by single vesicle analyses. *Earth Planet. Sci. Lett.* **449**, 145–154 (2016).
12. Mundl-Petermeier, A. et al. Anomalous ^{182}W in high ^{3}He/^{4}He ocean island basalts: fingerprints of Earth's core? *Geochim. Cosmochim. Acta* **271**, 194–211 (2020).
13. Kurz, M. D., Curtice, J., Fornari, D., Geist, D. & Moreira, M. Primitive neon from the center of the Galapagos hotspot. *Earth Planet. Sci. Lett.* **286**, 23–34 (2009).
14. Mukhopadhyay, S. Early differentiation and volatile accretion recorded in deep-mantle neon and xenon. *Nature* **486**, 101–104 (2012).
15. Trieloff, M., Kunz, J., Clague, D. A., Harrison, D. & Allègre, C. J. The nature of pristine noble gases in mantle plumes. *Science* **288**, 1036–1038 (2000).
16. Harrison, D., Burnard, P. & Turner, G. Noble gas behaviour and composition in the mantle: constraints from the Iceland Plume. *Earth Planet. Sci. Lett.* **171**, 199–207 (1999).
17. Render, J., Fischer-Gödde, M., Burkhardt, C. & Kleine, T. The cosmic molybdenum–neodymium isotope correlation and the building material of the Earth. *Geochem. Perspect. Lett.* **3**, 170–178 (2017).
18. Akram, W., Schönbächler, M., Bisterzo, S. & Gallino, R. Zirconium isotope evidence for the heterogeneous distribution of s-process materials in the Solar System. *Geochim. Cosmochim. Acta* **165**, 484–500 (2015).
19. Hirschmann, M. M. & Dasgupta, R. The H/C ratios of Earth's near-surface and deep reservoirs, and consequences for deep Earth volatile cycles. *Chem. Geol.* **262**, 4–16 (2009).
20. Marty, B. The origins and concentrations of water, carbon, nitrogen and noble gases on Earth. *Earth Planet. Sci. Lett.* **313–314**, 56–66 (2012).
21. Marty, B. et al. Xenon isotopes in 67P/Churyumov–Gerasimenko show that comets contributed to Earth's atmosphere. *Science* **356**, 1069–1072 (2017).
22. Harper, C. L. & Jacobsen, S. B. Noble gases and Earth's accretion. *Science* **273**, 1814–1818 (1996).
23. O'Brien, D. P., Walsh, K. J., Morbidelli, A., Raymond, S. N. & Mandell, A. M. Water delivery and giant impacts in the 'grand tack' scenario. *Icarus* **239**, 74–84 (2014).
24. Meshik, A., Hohenberg, C., Pravdivtseva, O. & Burnett, D. Heavy noble gases in solar wind delivered by Genesis mission. *Geochim. Cosmochim. Acta* **127**, 326–347 (2014).
25. Busemann, H., Baur, H. & Wieler, R. Primordial noble gases in 'Phase Q' in carbonaceous and ordinary chondrites studied by closed-system stepped etching. *Meteorit. Planet. Sci.* **35**, 949–973 (2000).
26. Williams, C. D. & Mukhopadhyay, S. Capture of nebular gases during Earth's accretion is preserved in deep-mantle neon. *Nature* **565**, 78–81 (2019).
27. Yokochi, R. & Marty, B. A determination of the neon isotopic composition of the deep mantle. *Earth Planet. Sci. Lett.* **225**, 77–88 (2004).
28. French, S. W. & Romanowicz, B. Broad plumes rooted at the base of the Earth's mantle beneath major hotspots. *Nature* **525**, 95–99 (2015).
29. Ballentine, C. J. & Barfod, D. N. The origin of air-like noble gases in MORB and OIB. *Earth Planet. Sci. Lett.* **180**, 39–48 (2000).
30. Caffee, M. W. et al. Primordial noble gases from Earth's mantle: identification of primitive volatile component. *Science* **285**, 2115–2118 (1999).
31. Holland, G. & Ballentine, C. J. Seawater subduction controls the heavy noble gas composition of the mantle. *Nature* **441**, 186–191 (2006).
32. Bekaert, D. V., Broadley, M. W., Caracausi, A. & Marty, B. Novel insights into the degassing history of Earth's mantle from high precision noble gas analysis of magmatic gas. *Earth Planet. Sci. Lett.* **525**, 115766 (2019).
33. Parai, R. & Mukhopadhyay, S. The evolution of MORB and plume mantle volatile budgets: constraints from fission Xe isotopes in Southwest Indian Ridge basalts. *Geochem. Geophys. Geosyst.* **16**, 719–735 (2015).
34. Busemann, H. & Eugster, O. The trapped noble gas component in achondrites. *Meteorit. Planet. Sci.* **37**, 1865–1891 (2002).
35. Broadley, M. W., Bekaert, D. V., Marty, B., Yamaguchi, A. & Barrat, J.-A. Noble gas variations in ureilites and their implications for ureilite parent body formation. *Geochim. Cosmochim. Acta* **270**, 325–337 (2020).
36. Pető, M. K., Mukhopadhyay, S. & Kelley, K. A. Heterogeneities from the first 100 million years recorded in deep mantle noble gases from the Northern Lau Back-arc Basin. *Earth Planet. Sci. Lett.* **369–370**, 13–23 (2013).
37. Ott, U., Begemann, F., Yang, J. & Epstein, S. S-process krypton of variable isotopic composition in the Murchison meteorite. *Nature* **332**, 700–702 (1988).
38. Lewis, R. S., Amari, S. & Anders, E. Interstellar grains in meteorites: II. SiC and its noble gases. *Geochim. Cosmochim. Acta* **58**, 471–494 (1994).
39. Dauphas, N. The isotopic nature of the Earth's accreting material through time. *Nature* **541**, 521–524 (2017).
40. Pepin, R. O. & Porcelli, D. Xenon isotope systematics, giant impacts, and mantle degassing on the early Earth. *Earth Planet. Sci. Lett.* **250**, 470–485 (2006).
41. Pepin, R. O. On the origin and early evolution of terrestrial planet atmospheres and meteoritic volatiles. *Icarus* **92**, 2–79 (1991).
42. Carlson, R. W. et al. How did early Earth become our modern world? *Annu. Rev. Earth Planet. Sci.* **42**, 151–178 (2014).
43. Rubin, M. et al. Krypton isotopes and noble gas abundances in the coma of comet 67P/Churyumov–Gerasimenko. *Sci. Adv.* **4**, eaar6297 (2018).
44. Mazor, E., Heymann, D. & Anders, E. Noble gases in carbonaceous chondrites. *Geochim. Cosmochim. Acta* **34**, 781–824 (1970).
45. Heber, V. S. et al. Noble gas composition of the solar wind as collected by the Genesis mission. *Geochim. Cosmochim. Acta* **73**, 7414–7432 (2009).
46. Pahlevan, K. & Stevenson, D. J. Equilibration in the aftermath of the lunar-forming giant impact. *Earth Planet. Sci. Lett.* **262**, 438–449 (2007).
47. Lock, S. J. & Stewart, S. T. The structure of terrestrial bodies: Impact heating, corotation limits, and synestias. *J. Geophys. Res. Planets* **122**, 950–982 (2017).
48. Bekaert, D. V., Broadley, M. W. & Marty, B. The origin and fate of volatile elements on Earth revisited in light of noble gas data obtained from comet 67P/Churyumov–Gerasimenko. *Sci. Rep.* **10**, 5796 (2020).
49. Ciesla, F. J. & Cuzzi, J. N. The evolution of the water distribution in a viscous protoplanetary disk. *Icarus* **181**, 178–204 (2006).
50. Raymond, S. N. & Izidoro, A. Origin of water in the inner Solar System: planetesimals scattered inward during Jupiter and Saturn's rapid gas accretion. *Icarus* **297**, 134–148 (2017).

Methods

Samples

We used centimetre-sized basaltic glass chunks of samples AHA-NEMO2-D22A and AHA-NEMO2-D22B from a submarine lava flow of Fernandina Volcano, Galápagos[13,51]. The composition of these samples for major, trace and volatile (major and noble gases) elements have been well characterized[11,13,51,52]. In particular, these samples have the most primitive He and Ne isotopic ratios of the Galápagos hotspot[11,13].

The Iceland sample DG2017 is a picritic subglacial basalt glass from Dagmalafell (Midfell), located approximately 1 km east of Lake Þingvallavatn. The GPS coordinates are 64° 10′ 29.3″ N, 21° 02′ 52.1″ W. This sample was collected by Adam Kent in 2017 from the same locality as the DICE10 sample analysed previously[16], from a small quarry at the base of a hill formed by subglacial eruptions. The sample material was taken from a mass of pillow basalts, more than 50 m high that underlies hyaloclastite. Abundances of CO_2 and He as well as the He isotopic ratio for sample DG2017, measured by crushing and melting at Oregon State University (OSU)[53], are shown in Supplementary Table 1, and are consistent with previous studies[14–16,54]. The He isotope ratio of DICE10, as measured at OSU, is the same within uncertainties as measured for the DG2017 sample. Abundances and isotopic compositions of Ne, Ar and Xe have also been reported for this locality[14–16,54].

Glass chunks from Galápagos and Iceland were cleaned in oxalic acid (1%) on a hot plate (50 °C) and then rinsed with ethanol and acetone in ultrasonic baths. About 4 g (Extended Data Table 1, Supplementary Table 2) of each sample was then put into crushers, which were then baked between 110 °C and 120 °C for 24 h and pumped for a minimum of 4 weeks before starting the analyses. Analyses were started when the crusher blanks were below 1.0×10^{-13} ccSTP (cm^3 at standard temperature and pressure) of ^{22}Ne, 4.6×10^{-12} ccSTP of ^{36}Ar, 4.5×10^{-14} ccSTP of ^{84}Kr and 1.1×10^{-15} ccSTP of ^{130}Xe.

Protocol of accumulation and noble gas purification

We used a recently developed accumulation protocol[8], consisting of accumulating heavy noble gases (Ar, Kr and Xe) only for crushing steps showing little atmospheric contamination as determined by the prior analyses of neon isotopic ratios $^{20}Ne/^{22}Ne$ and $^{21}Ne/^{22}Ne$.

For each crushing step, gases were first purified successively with a hot (400 °C) MP10 SAES getter and then with a cold (room temperature) MP10 SAES getter. After purification, gases were trapped on a dual cryogenic trap[55]. The latter is a new cryogenic system composed of two electropolished stainless steel traps on one cold head[55]. One trap can be cooled to <5 K (hereafter trap A) and the other trap to <50 K (hereafter trap B). The nude stainless-steel traps present steeper release curves for noble gases than charcoal traps[56], allowing a better Ar/Kr/Xe separation[55].

Noble gases, except He, were then trapped on trap A at 9 K. A temperature cycle of the trap was then conducted, consisting of putting the trap at 35 K for 5 min and then cooling it to 9 K. This temperature cycle is effective in limiting the effect of cryotrapping (the process by which one noble gas is trapped by another one) as it can better re-layer each noble gas under each other on the trap[57]. This operation allows recovery of a higher fraction of each noble gas. Neon was then released at 25 K and introduced to the Noblesse mass spectrometer for analysis (see below).

If the $^{20}Ne/^{22}Ne$ ratio of the crushing step was higher than 11.75 (and 11.49 for one step, Supplementary Table 2), then the heavy noble gases on trap A were released at 160 K and trapped on a charcoal trap at liquid nitrogen temperature (77 K) for accumulation.

To analyse the composition of the accumulated gas, the charcoal trap was first heated with a Kapton heater at 40 °C to release all the Xe. The accumulated gas was first purified with the two hot and cold MP10 SAES getters. Then gases were trapped on trap B at 67 K. The protocol then used to separate Ar/Kr/Xe was protocol 2 described in another study[55] for samples D22B-1, D22B-1 and DG2017-1. For the three other analyses, two temperature cycles were applied for Ar/Kr and Kr/Xe separation (similar to protocol 3 of a previous study[55]) to further improve the efficiency of the separation.

The Ne, Ar and Xe data for the samples are indicated in Extended Data Tables 2, 4 and Supplementary Table 2.

The charcoal trap, used to accumulate Ar, Kr and Xe from several crushing steps (Supplementary Table 2), remained in a static vacuum for several days. In total, the charcoal trap remained in a static vacuum for 6 days (isolated) for sample D22B-1, 5 days for D22B-2, 5 days for D22B-3, 3 days for D22A, 7 days for DG2017-1 and 3 days for DG2017-2. The blank of the charcoal trap after several days in a static vacuum is discussed below.

Noble gas analyses on the Noblesse 5F5M

To measure the noble gas abundances and isotopic ratios, we use a Noblesse HR mass spectrometer (Nu Instruments) equipped with five Faraday cups and five electron multipliers (5F5M) at the Davis Noble Gas Laboratory. The filament voltage was kept at −78 V and the trap current was kept at 250 μA for all the analyses.

Neon isotopes—^{20}Ne, ^{21}Ne and ^{22}Ne—were measured in multicollection on electron multipliers, on the right side of the peaks where ^{20}Ne is resolved from $^{40}Ar^{++}$. Signals of hydrofluoric acid (HF) and at mass 44 were measured to correct for HF^+ and CO_2^{++} interferences, using the measured double/single charge ratios CO_2^{++}/CO_2^{+} of 0.0068 ± 0.0005.

The Ar isotopes were measured in multicollection, ^{40}Ar on one of the Faraday cups and ^{36}Ar and ^{38}Ar on electron multipliers.

The Kr isotopes were measured in two steps on electron multipliers. The first step consisted of measuring ^{78}Kr, ^{80}Kr, ^{82}Kr, ^{84}Kr and ^{86}Kr in multicollection, and the second step consisted of analysing ^{83}Kr. Measurements were done on the left side of the peaks, where interferences with hydrocarbon on Kr isotopes are resolved. The isotope ^{80}Kr was measured on the electron multiplier that has a slit (initially for resolving ^{3}He from HD) that allows full resolution of ^{80}Kr from any interfering hydrocarbons. Kr is efficiently separated from Ar using the dual stainless steel trap[55]. As a result, no interference of $^{40}Ar_2^{+}$ with ^{80}Kr was detected (see discussion below).

The Xe isotopes were measured in three steps on electron multipliers, the first step for ^{126}Xe, ^{129}Xe and ^{132}Xe, the second step for ^{128}Xe, ^{131}Xe and ^{134}Xe and the third step for ^{124}Xe, ^{130}Xe and ^{136}Xe.

Sensitivity, reproducibility and mass discrimination of the measurements

Sensitivity, reproducibility and mass discrimination of the measurements were assessed through repeat analyses of air standards of similar size to the samples. Each pipette of the air standard corresponds to 6.15×10^{-11} ccSTP of ^{22}Ne, 1.15×10^{-9} ccSTP of ^{36}Ar, 2.38×10^{-11} ccSTP of ^{84}Kr and 1.30×10^{-13} ccSTP of ^{130}Xe.

Typical values of sensitivity of the mass spectrometer during the analysis periods were 1.1×10^{-14} cm^3 c.p.s.$^{-1}$ for ^{22}Ne, 1.9×10^{-15} cm^3 c.p.s.$^{-1}$ for ^{36}Ar, 4.8×10^{-16}–5.0×10^{-16} cm^3 c.p.s.$^{-1}$ for ^{84}Kr and 4.6×10^{-16}–5.1×10^{-16} cm^3 c.p.s.$^{-1}$ for ^{130}Xe.

Extended Data Fig. 4 shows the measurement reproducibility of air standards of three different sizes, from 7.52×10^{-12} cm^3 to 2.38×10^{-11} cm^3 of ^{84}Kr. For data reduction, only air standards of similar size to the samples were considered. Repeat measurements of the largest air standard size (^{84}Kr of 2.38×10^{-11} cm^3) show an even better reproducibility, typically of 2‰ for $^{78}Kr/^{84}Kr$, of 2.5‰ for $^{80}Kr/^{84}Kr$, of 1‰ for $^{82}Kr/^{84}Kr$, of 1.5‰ for $^{83}Kr/^{84}Kr$ and of 1‰ for $^{86}Kr/^{84}Kr$.

Accumulation blank and tests

An important parameter to monitor is the blank of the charcoal trap (see above the total numbers of days the trap remained in a static vacuum for each sample). We carried out accumulation blanks consisting of trapping Ar, Kr and Xe from the line in different blank steps,

as we did for the crush steps. The accumulated blank represents 3.1% of the total measured Kr for sample D22B-1, 1.7% for D22B-2, 1.9% for D22B-3, 3.7% for D22A, 2.1% for DG2017-1 and 1.9% for DG2017-2, with atmospheric isotopic ratios. These blanks represent 3.2% and 6.7% of the total measured Ar and Xe, respectively, for sample D22B-1, 1.9% and 3.7% for D22B-2, 2.1% and 4.0% for D22B-3, 3.6% and 8.0% for D22A, 3.8% and 4.8% for DG2017-1 and 1.9% and 4.0% for DG2017-2. We corrected the measured Ar, Kr and Xe abundances and isotopic ratios for these blanks. This correction is negligible given the blank proportions for each sample.

The measured Kr isotopic ratios for the D22 and DG2017 samples are similar, within uncertainties, suggesting that the blank correction is not important for this accumulation procedure, that is, the quantity of accumulated gas is too large to be affected by the blank. These similar results provide confidence that the procedure is reproducible for precisely measuring small variations in Kr isotopes in such samples despite the considerable amount of gas processing/distillations.

However, the measured Kr and Xe isotopic ratios may be lower limits for the Galápagos and Iceland sources, as for the accumulation protocol we considered crushing steps with $^{20}Ne/^{22}Ne$ lower than the maximum measured value for these sources. The average $^{20}Ne/^{22}Ne$ ratios of the accumulated gas for each sample are between 11.99 and 12.41 (Supplementary Table 2), which is lower than the maximum measured value of more than 12.8 for these sources. However, as explained in a previous study[8], mixing in a Kr–Ne or Xe–Ne space would be hyperbolic and so crushing steps with lower $^{20}Ne/^{22}Ne$ ratio than the maximum value but higher than 11.75 would still have Kr and Xe isotopic ratios very close to the source value (Extended Data Fig. 2). Therefore, we expect the measured Kr and Xe isotopic ratios to be representative of the Galápagos and Iceland sources. As there are no previous Kr isotopic data for a high $^{20}Ne/^{22}Ne$ ratio for these oceanic islands, we cannot correct for this small effect.

In addition, we note that the small Kr isotopic differences observed between the four D22 and the two DG2017 measurements may be explained either by instrumental variability (as observed with standards) or by small differences in the air-like contaminant (air versus seawater, for instance). More investigation would be needed to determine the cause of these small variations.

The Ne isotopic ratios fall exactly on the mixing lines previously determined for these samples in other noble gas labs (Supplementary Table 2). This is a further confirmation of the robustness of the measurements by the new 5F5M mass spectrometer. Another important observation is that the measured $^{40}Ar/^{36}Ar$ ratios and the average $^{20}Ne/^{22}Ne$ ratios of the accumulated gas fall exactly on the mixing hyperbolae previously identified for these samples (Extended Data Fig. 5). The $^{129}Xe/^{130}Xe$ and $^{136}Xe/^{130}Xe$ ratios also fall exactly on the trend identified for Iceland[14] (Fig. 3), but there are no previously published data for the Galápagos hotspot samples. This is robust evidence that suggests that the accumulation protocol worked very well for these samples and that the measured Kr isotopic ratios are representative of these OIB sources. In Fig. 3b, data for upper mantle include MORB from the North Atlantic[8,58–60], the equatorial Atlantic[61] and the South West Indian Ridge[33,62], CO_2 well gas[31], and thermal springs from Eifel[32] and Massif Central[63].

However, the Ar abundances and Ar isotopic ratios cannot be taken as representative of the source compositions. As shown in Extended Data Fig. 5, the measured $^{40}Ar/^{36}Ar$ ratios with the accumulation protocol are much lower than the highest values determined for these samples. This is due to the principles of the accumulation protocol[8]: mixing in Extended Data Fig. 5 is hyperbolic and so accumulating steps with high $^{20}Ne/^{22}Ne$ ratios (greater than 11.75) provides Kr with similar isotopic ratios as the source but Ar with much lower ratios.

We also carried out tests of accumulation with aliquots of air standard. For each of the three tests, three aliquots of 7.52×10^{-12} cc of ^{84}Kr were accumulated on the charcoal trap and analysed as explained above. The measured Kr isotopic ratios for each test, presented in Extended Data Table 5, are similar to measurements of air standard aliquots of 7.52×10^{-12} cc and of 2.37×10^{-11} cc of ^{84}Kr. The results of these tests argue against mass fractionation induced by the accumulation protocol itself.

Uncertainties on isotopic ratios and discussion of the results

The uncertainties on isotopic ratios were calculated by propagation of errors of the measured uncertainty and of the external reproducibility estimated with standards. For each sample, the external reproducibility was estimated by considering a suite of air standards, with similar size to the samples (as explained above), analysed before and after the sample.

The $^{86}Kr/^{84}Kr$ ratios were not corrected for fission production, as it is expected to be negligible. Spontaneous fission of ^{238}U can produce small amounts of ^{83}Kr, ^{84}Kr and ^{86}Kr whereas spontaneous fission of ^{244}Pu produces ^{86}Kr (ref. [64]). The fission yields are 0.95% and 0.11% for ^{86}Kr from ^{238}U and ^{244}Pu fissions, respectively[64]. It is important to note that this correction would lower the measured $^{86}Kr/^{84}Kr$ ratio. Therefore, the anomaly observed for ^{86}Kr (Figs. 1, 5) would be even more important with this fissiogenic correction.

Another observation that precludes interference on ^{80}Kr from $^{40}Ar_2^+$ is the overall pattern in Fig. 1. As the Kr isotopic pattern closely follows that of Phase Q for isotopes of mass 78, 80, 82 and 83, it is unlikely that any interference with $^{40}Ar_2^+$ on mass 80 occurred. Otherwise, we should observe a noticeable excess for the $^{80}Kr/^{84}Kr$ ratio relative to Phase Q.

We also estimated the probabilities that the measured Kr isotopic ratios are identical to air within uncertainties. Considering the six data independently, we calculated the probability that the $^{78}Kr/^{84}Kr$, $^{80}Kr/^{84}Kr$ and $^{82}Kr/^{84}Kr$ ratios are all identical to or higher than air by randomly picking an isotopic ratio based on the measured value and the uncertainty assuming a normal distribution, and comparing it with the atmospheric ratios, also randomly picked according to the normal distribution. We found that the probability that the $^{78}Kr/^{84}Kr$, $^{80}Kr/^{84}Kr$ and $^{82}Kr/^{84}Kr$ ratios are all identical to or higher than air is 0.19% for sample D22B-1, 0% for samples D22B-2, D22B-3 and D22A, 2.19% for DG2017-1 and 0.38% for DG2017-2. Similarly, the probabilities that the $^{78}Kr/^{84}Kr$, $^{80}Kr/^{84}Kr$ and $^{82}Kr/^{84}Kr$ ratios are all within uncertainties of air ($\pm 2\sigma$) are 0.23% for sample D22B-1, 0.12% for D22B-2, 0% for D22B-3, 0.66% for D22A, 1.5% for DG2017-1 and 0.21% for DG2017-2. The probabilities that all five Kr isotopic ratios are within uncertainties of air ($\pm 2\sigma$) are 0.09% for sample D22B-1, 0.002% for D22B-2, 0% for D22B-3, 0.24% for D22A, 0.37% for DG2017-1 and 0.07% for DG2017-2. Therefore, these calculations demonstrate that it is very likely that the measured Kr isotopic compositions are different from air.

Kr cosmochemistry and compilation of chondrites Kr isotopic data

The Kr isotopic composition of carbonaceous chondrites is a mixture of Phase Q Kr and Kr from presolar grains such as SiC, which were used to determine the slow-process Kr isotopic composition[37,38]. The large variability in $\delta^{86}Kr$ of SiC grains are due to the fact that ^{86}Kr is at a branching point on the slow-process path and thus the SiC grain composition is influenced by neutron flux and stellar temperature in individual AGB stars. The Kr isotopic compositions of SiC grains reflect mixtures of the normal 'N' component, close to the solar composition, and the 'G' component, corresponding to slow-process Kr, and the range in Kr isotopic ratios is predicted by AGB star composition models[38].

We compiled Kr isotopic data from carbonaceous, ordinary and enstatite chondrites (Extended Data Table 3) to compare with our data. We report data only for chondrites of low petrologic types (1 to 3) as they have better preserved their original constituents[65].

We re-determined the AVCC Kr isotopic composition (Extended Data Tables 1, 3) to take into account more data than usually considered and also because it is not always clear in the literature from which data this AVCC composition was calculated. It is often referred for AVCC to the study of Pepin[66] but in this study chondritic Kr is not only calculated with data for carbonaceous chondrites.

For the calculation of AVCC, we used data from several studies that have measured the carbonaceous chondrites Murray, Cold Bokkeveld, Orgueil, Lancé and Leoville[67–70]. Some data were not considered because some meteorites were too much affected by Kr from neutron-capture production[71,72].

All the data considered were first re-normalized to the atmospheric composition used in this study[73] in case other values were taken. The data for Leoville[69] were corrected considering they were reported to the atmospheric composition of Nier[74] as described in the data table, and not to that of Nief[75] as mentioned in the text.

The data for Leoville[69] were corrected for cosmogenic Kr production, for the other carbonaceous meteorites no cosmogenic correction appears necessary[67,68,70]. To correct Leoville data for cosmogenic Kr, we use two methods that give similar results. The first one consisted of using the $^{78}Kr/^{21}Ne$ ratio of the spallation end-member[76] of 7.6×10^{-6} and the Kr spallation spectra[77]. The second method consisted of calculating the production ratios of $^{83}Kr/^{21}Ne$ for the spallogenic end-member on the basis of determined equations[78] provided that $^{22}Ne/^{21}Ne > 1.08–1.10$ (refs. [78,79]) and combining this production ratio with the Kr spallation spectra[77]. The correction was less than 0.2% for all isotopic ratios. The data were not corrected for neutron-capture production.

The AVCC composition calculated in Extended Data Table 3 represents the weighted mean of the eight data considered (only five data for ^{78}Kr and six for ^{80}Kr). The uncertainties reported are the standard error of the mean to take into account the underdispersion/overdispersion of the data. We note that because Earth accreted substantial amounts of carbonaceous meteorites (approximately 5–15% of bulk Earth mass[5,39]), the average value of the carbonaceous meteorites (AVCC) should be representative of the composition of the carbonaceous meteorites accreted. Consequently, the appropriate parameter for the uncertainty of the average value is the standard error. Our calculated mean value for AVCC composition is consistent with a previous estimation[67].

For ordinary chondrites, we selected data from the study of Eugster[80] (Extended Data Table 3), and corrected them for cosmogenic production using their estimated $^{83}Kr/^{21}Ne$ (ref. [80]) and the Kr spallation spectra[77]. We did not report the $^{80}Kr/^{84}Kr$ and $^{82}Kr/^{84}Kr$ ratios as both ratios are clearly affected by neutron-induced production.

For enstatite chondrites, we used data from two studies[81,82] and corrected them for cosmogenic production using the Kr spallation spectra[77] and the calculated production ratios $^{83}Kr/^{21}Ne$ for the spallogenic end-member[78]. We report only the $^{83}Kr/^{84}Kr$ and $^{86}Kr/^{84}Kr$ ratios, as the other isotopic ratios show more variability, probably owing to imperfect neutron-induced production correction for $^{80}Kr/^{84}Kr$ and $^{82}Kr/^{84}Kr$ ratios and to imperfect cosmogenic correction for the $^{78}Kr/^{84}Kr$ ratio.

As for AVCC, the averages for enstatite and ordinary chondrites correspond to the weighted mean and the reduced chi-square of the weighted error.

Calculation of the Kr mixing proportions in the OIB sources

To explain the Kr isotopic patterns of the Galápagos and Iceland sources, we considered several mixing combinations (Fig. 4). The aim of this approach was to fit the anomalies in $^{78}Kr/^{84}Kr$ and $^{80}Kr/^{84}Kr$, the two ratios most resolvable from the air ratios, to estimate the expected $^{86}Kr/^{84}Kr$ ratio. We used the same methods of linear least square fitting and Monte Carlo for propagation of uncertainties as described for Xe component deconvolution[33].

If the composition of Kr in the plume sources is a mixture of AVCC and atmospheric Kr, then 52 ± 8% of the Kr in the Galápagos plume and 36 ± 8% of the Kr in the Iceland plume originate from AVCC on the basis of the measured $^{78}Kr–^{80}Kr–^{84}Kr$. A solar–AVCC mixture would indicate that at most 10 ± 2% of the Kr in the Galápagos plume and 16 ± 2% of the Kr in the Iceland plume would be solar. A Phase Q–air mixture would give 100^{0}_{-9}% and 71 ± 17% of the Kr in the Galápagos and Iceland plumes, respectively, originated from Q.

We also tested this approach considering a mixing of AVCC, solar and air Kr to fit the $^{78}Kr/^{84}Kr$, $^{80}Kr/^{84}Kr$ and $^{82}Kr/^{84}Kr$ ratios. This three-component mixing gives a similar result for samples D22 to the mixing of AVCC–air Kr, that is, 0% of solar Kr, 48 ± 6% of AVCC Kr and 52 ± 6% of air Kr. However, it was not possible to fit well the DG2017 sample composition with this three-component mixing given that the measured $^{82}Kr/^{84}Kr$ ratio for this sample is not as well resolved from air as for samples D22. The fact that this three-component mixing gives the same result as the two-component mixing considering only the $^{78}Kr/^{84}Kr$ and $^{80}Kr/^{84}Kr$ ratios for samples D22 suggests that it is a valid approach to only consider these two ratios for the fit and that the solar end-member did not contribute substantially to mantle Kr.

The uncertainties on the mixing proportions take into account uncertainties on the measured Kr isotopic ratios for the samples as well as the uncertainties on the AVCC, solar and Phase Q end-members.

Data availability

The geochemical data that support the findings of this study are archived on EarthChem at https://ecl.earthchem.org/view.php?id=2065. Source data are provided with this paper.

51. Geist, D. et al. Submarine Fernandina: magmatism at the leading edge of the Galapagos hot spot. *Geochem. Geophys. Geosyst.* **7**, Q12007 (2006).
52. Peterson, M. E. et al. Submarine basaltic glasses from the Galapagos Archipelago: determining the volatile budget of the mantle plume. *J. Petrol.* **58**, 1419–1450 (2017).
53. Graham, D. W., Hanan, B. B., Hémond, C., Blichert-Toft, J. & Albarède, F. Helium isotopic textures in Earth's upper mantle. *Geochem. Geophys. Geosyst.* **15**, 2048–2074 (2014).
54. Colin, A., Moreira, M., Gautheron, C. & Burnard, P. Constraints on the noble gas composition of the deep mantle by bubble-by-bubble analysis of a volcanic glass sample from Iceland. *Chem. Geol.* **417**, 173–183 (2015).
55. Péron, S., Mukhopadhyay, S. & Huh, M. A new dual stainless steel cryogenic trap for efficient separation of krypton from argon and xenon. *J. Analyt. At. Spectrom.* **35**, 2663–2671 (2020).
56. Lott, D. E. III Improvements in noble gas separation methodology: a nude cryogenic trap. *Geochem. Geophys. Geosyst.* **2**, 1068 (2001).
57. Stanley, R. H. R., Baschek, B., Lott, D. E. III & Jenkins, W. J. A new automated method for measuring noble gases and their isotopic ratios in water samples. *Geochem. Geophys. Geosyst.* **10**, Q05008 (2009).
58. Kunz, J., Staudacher, T. & Allègre, C. J. Plutonium-fission xenon found in Earth's mantle. *Science* **280**, 877–880 (1998).
59. Moreira, M., Kunz, J. & Allègre, C. J. Rare gas systematics on popping rock: estimates of isotopic and elemental compositions in the upper mantle. *Science* **279**, 1178–1181 (1998).
60. Parai, R. & Mukhopadhyay, S. Heavy noble gas signatures of the North Atlantic Popping Rock 2ΠD43: implications for mantle noble gas heterogeneity. *Geochim. Cosmochim. Acta* **294**, 89–105 (2021).
61. Tucker, J. M., Mukhopadhyay, S. & Schilling, J.-G. The heavy noble gas composition of the depleted MORB mantle (DMM) and its implications for the preservation of heterogeneities in the mantle. *Earth Planet. Sci. Lett.* **355–356**, 244–254 (2012).
62. Parai, R., Mukhopadhyay, S. & Standish, J. J. Heterogeneous upper mantle Ne, Ar and Xe isotopic compositions and a possible Dupal noble gas signature recorded in basalts from the Southwest Indian Ridge. *Earth Planet. Sci. Lett.* **359–360**, 227–239 (2012).
63. Moreira, M., Rouchon, V., Muller, E. & Noirez, S. The xenon isotopic signature of the mantle beneath Massif Central. *Geochem. Perspect. Lett.* **6**, 28–32 (2018).
64. Ozima, M. & Podosek, F. A. *Noble Gas Geochemistry* (Cambridge Univ. Press, 2002).
65. Huss, G. R. & Lewis, R. S. Presolar diamond, SiC, and graphite in primitive chondrites: abundances as a function of meteorite class and petrologic type. *Geochim. Cosmochim. Acta* **59**, 115–160 (1995).
66. Pepin, R. O. On noble gas processing in the solar accretion disk. *Space Sci. Rev.* **106**, 211–230 (2003).
67. Eugster, O., Eberhardt, P. & Geiss, J. Krypton and xenon isotopic composition in three carbonaceous chondrites. *Earth Planet. Sci. Lett.* **3**, 249–257 (1967).
68. Marti, K. Isotopic composition of trapped krypton and xenon in chondrites. *Earth Planet. Sci. Lett.* **3**, 243–248 (1967).
69. Manuel, O. K., Wright, R. J., Miller, D. K. & Kuroda, P. K. Heavy noble gases in Leoville: The case for mass fractionated xenon in carbonaceous chondrites. *J. Geophys. Res.* **75**, 5693–5701 (1970).
70. Krummenacher, D., Merrihue, C. M., Pepin, R. O. & Reynolds, J. H. Meteoritic krypton and barium versus the general isotopic anomalies in meteoritic xenon. *Geochim. Cosmochim. Acta* **26**, 231–249 (1962).
71. Manuel, O. K., Wright, R. J., Miller, D. K. & Kuroda, P. K. Isotopic compositions of rare gases in the carbonacaous chondrites Mokoia and Allende. *Geochim. Cosmochim. Acta* **36**, 961–983 (1972).
72. Matsuda, J.-I., Lewis, R. S., Takahashi, H. & Anders, E. Isotopic anomalies of noble gases in meteorites and their origins—VII. C3V carbonaceous chondrites. *Geochim. Cosmochim. Acta* **44**, 1861–1874 (1980).
73. Basford, J. R., Dragon, J. C., Pepin, R. O., Coscio, M. R. Jr & Murthy, V. R. Krypton and xenon in lunar fines. *Lunar Planet. Sci. Proc.* **4**, 1915–1955 (1973).

74. Nier, A. O. A redetermination of the relative abundances of the isotopes of neon, krypton, rubidium, xenon and mercury. *Phys. Rev.* **79**, 450–454 (1950).
75. Nief, G. *Isotopic Abundance Ratios Given for Reference Samples Stocked by the National Bureau of Standards* (ed. Mohler, F.) NBS Technical Note 51 (National Bureau of Standards, 1960).
76. Eugster, O., Eberhardt, P. & Geiss, J. The isotopic composition of krypton in unequilibrated and gas rich chondrites. *Earth Planet. Sci. Lett.* **2**, 385–393 (1967).
77. Marti, K., Eberhardt, P. & Geiss, J. Spallation, fission, and neutron capture anomalies in meteoritic krypton and xenon. *Z. Naturforsch. A* **21**, 398–426 (1966).
78. Eugster, O. Cosmic-ray production rates for ^{3}He, ^{21}Ne, ^{38}Ar, ^{83}Kr, and ^{126}Xe in chondrites based on ^{81}Kr–Kr exposure ages. *Geochim. Cosmochim. Acta* **52**, 1649–1662 (1988).
79. Wieler, R. Cosmic-ray-produced noble gases in meteorites. *Rev. Mineral. Geochem.* **47**, 125–170 (2002).
80. Eugster, O., Eberhardt, P. & Geiss, J. Isotopic analyses of krypton and xenon in fourteen stone meteorites. *J. Geophys. Res.* **74**, 3874–3896 (1969).
81. Nakashima, D. & Nakamura, T. Trapped noble gas components and exposure history of the enstatite chondrite ALH84206. *Geochem. J.* **40**, 543–555 (2006).
82. Okazaki, R., Takaoka, N., Nagao, K. & Nakamura, T. Noble gases in enstatite chondrites released by stepped crushing and heating. *Meteorit. Planet. Sci.* **45**, 339–360 (2010).
83. Heber, V. S. et al. Isotopic fractionation of solar wind: evidence from fast and slow solar wind collected by the Genesis Mission. *Astrophys. J.* **759**, 121–133 (2012).
84. Pepin, R. O., Schlutter, D. J., Becker, R. H. & Reisenfeld, D. B. Helium, neon, and argon composition of the solar wind as recorded in gold and other Genesis collector materials. *Geochim. Cosmochim. Acta* **89**, 62–80 (2012).

Acknowledgements We thank M. Huh for assistance in the lab; and M. Huyskens, S. Stewart and S. J. Lock for helpful discussions and comments on the manuscript. The He isotope analyses in the OSU noble gas lab were supported by NSF 1763255. The collection of the Fernandina samples and WHOI participation was supported by NSF Ocean Sciences.

Author contributions S.P. and S.M. designed the study. S.P. carried out the noble gas (Ne, Ar, Kr and Xe) analyses, interpreted the data and wrote the manuscript with feedback from S.M. M.D.K. and D.W.G. provided the samples, discussed the results and contributed to the final manuscript preparation. D.W.G. carried out the He and CO_2 analyses of sample DG2017.

Competing interests The authors declare no competing interests.

Additional information

Supplementary information The online version contains supplementary material available at https://doi.org/10.1038/s41586-021-04092-z.
Correspondence and requests for materials should be addressed to Sandrine Péron.
Peer review information *Nature* thanks Hirochika Sumino and the other, anonymous, reviewer(s) for their contribution to the peer review of this work.

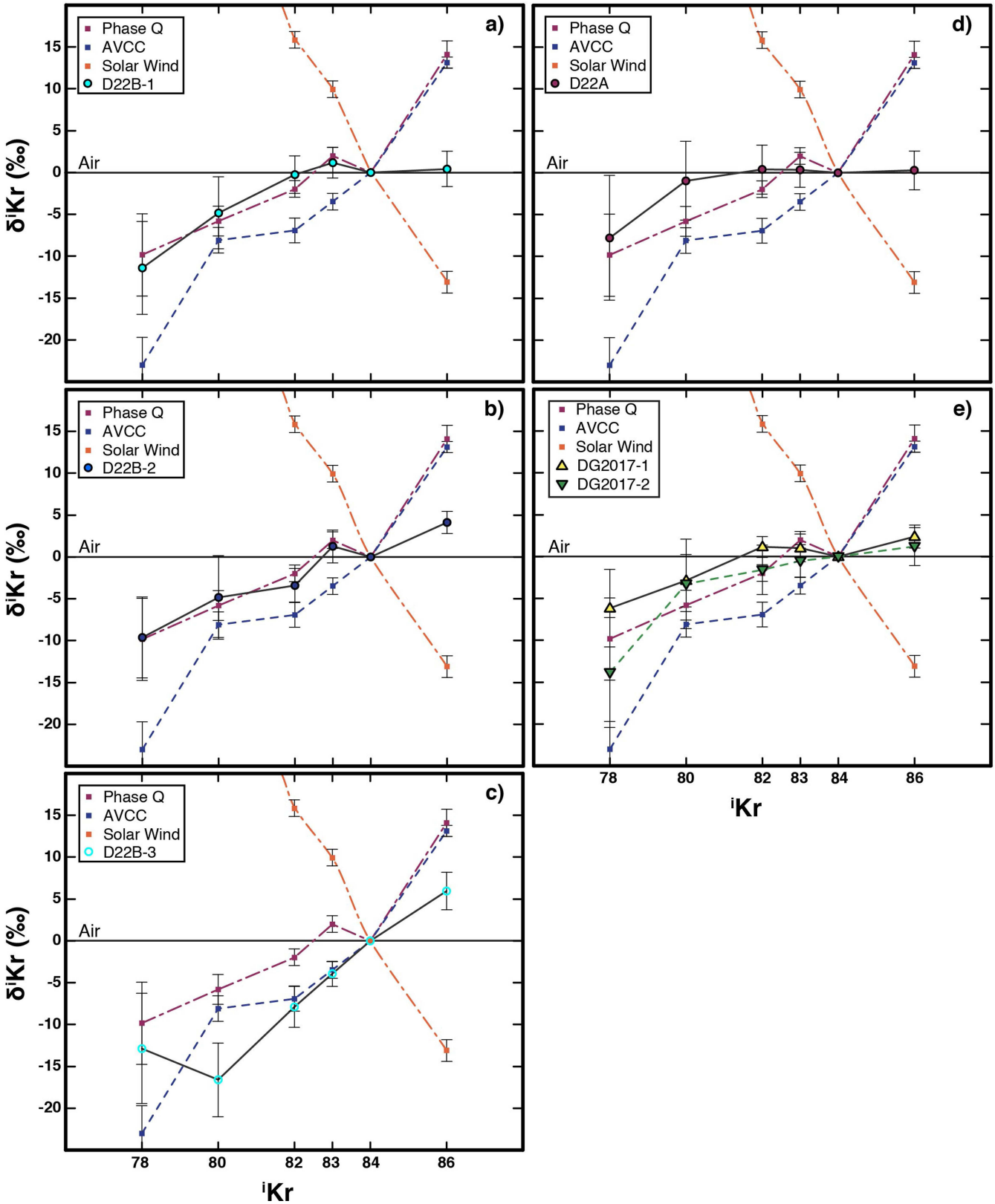

Extended Data Fig. 1 | Krypton isotopic patterns for each analysis. Isotopic ratios are in delta notation $\delta^{i}\mathrm{Kr} = ((^{i}\mathrm{Kr}/^{84}\mathrm{Kr})_{sample}/(^{i}\mathrm{Kr}/^{84}\mathrm{Kr})_{air} - 1) \times 10^{3}$. **a**, Sample D22B-1. **b**, Sample D22B-2. **c**, Sample D22B-3. **d**, Sample D22A. **e**, Samples DG2017-1 and DG2017-2. Patterns of solar wind[24], AVCC and Phase Q[25] are shown for reference.

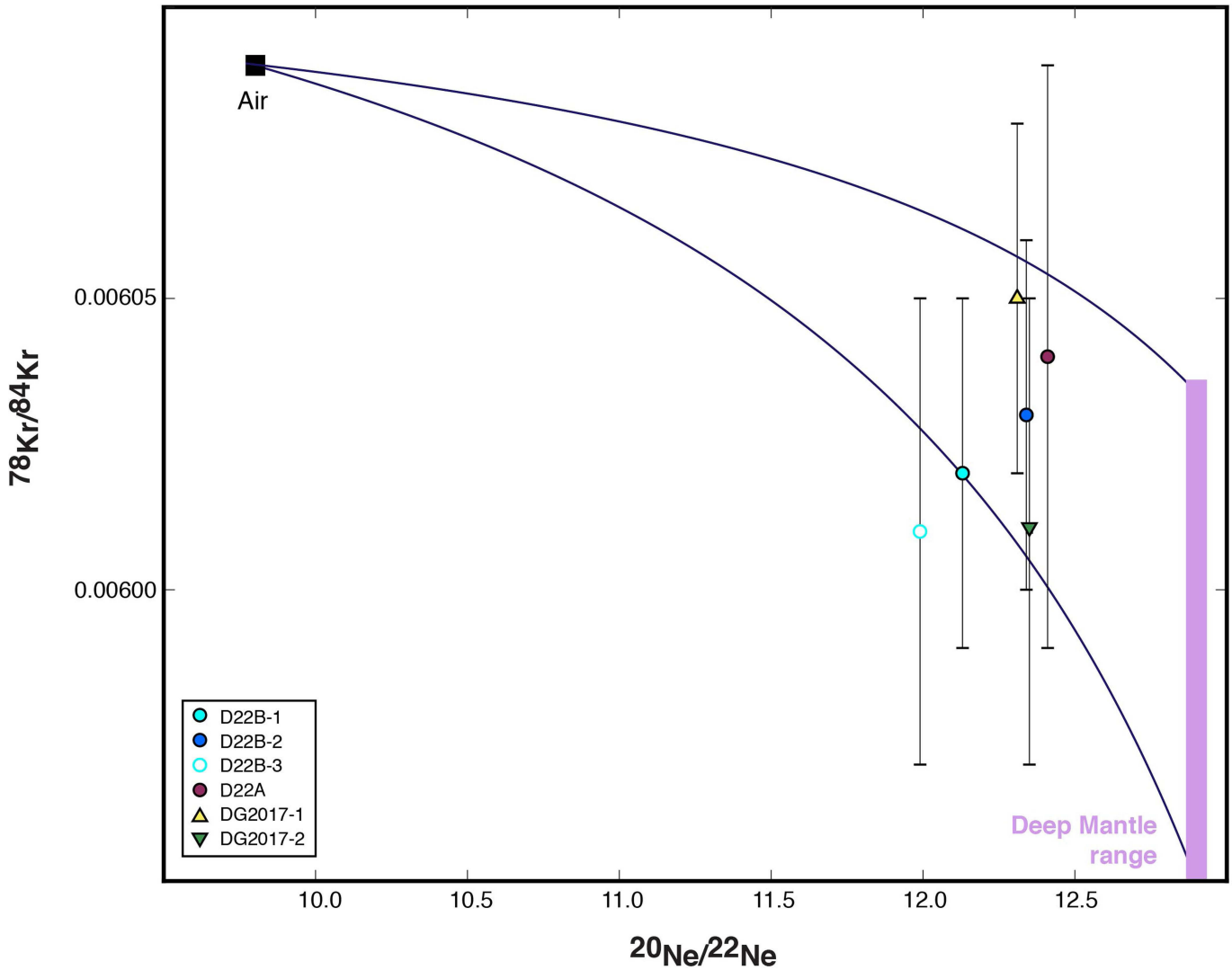

Extended Data Fig. 2 | Krypton–neon isotope plot. The krypton isotopic compositions of the Galápagos and Iceland mantle sources are not precisely known; our data represent a lower limit as explained in Methods. As such, a range is indicated for the deep mantle spanning the Phase Q and AVCC Kr isotopic compositions. The mixing hyperbolae show that accumulating crushing steps with $^{20}Ne/^{22}Ne$ ratios >11.75 allow to obtain Kr isotopic ratios close to the mantle source ratios.

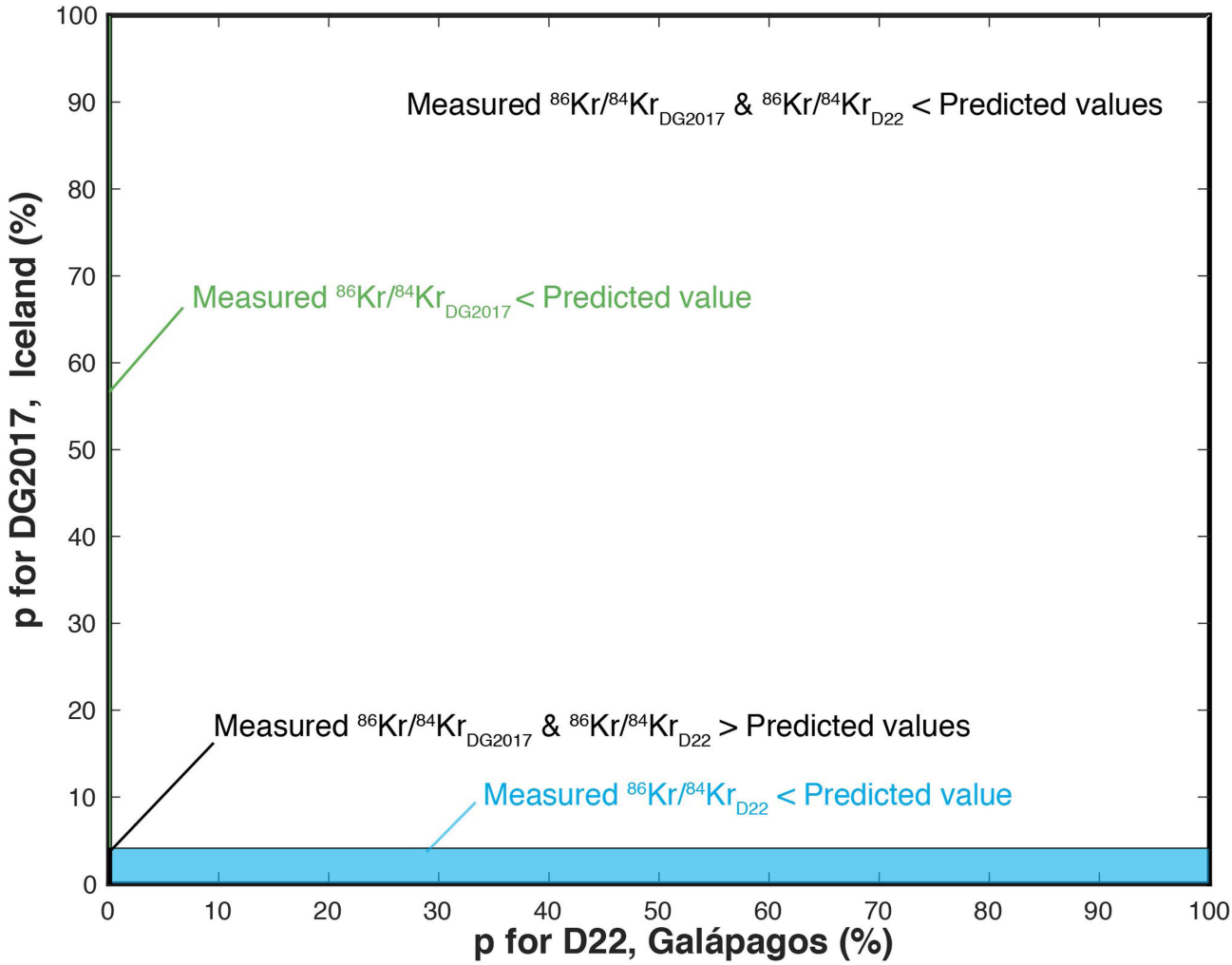

Extended Data Fig. 3 | Estimation of the probability of the observed deficit in ^{86}Kr for the D22 (Galápagos) and DG2017 (Iceland) samples. The black rectangle represents the probability (0.01%) that both measured ^{86}Kr/^{84}Kr ratios for the Galápagos and Iceland plume sources are higher than the predicted values (Fig. 5). The white rectangle represents the probability that both measured ratios are lower than the predicted values, the blue rectangle that the measured ratio for the Galápagos source is lower than the predicted value with the measured ratio for Iceland being higher than the predicted value, and the green rectangle that the measured ratio for the Iceland source is lower than the predicted value with the measured ratio for Galápagos being higher than the predicted value. There is a 99.9% probability that Earth's deep mantle has a deficit in ^{86}Kr relative to AVCC.

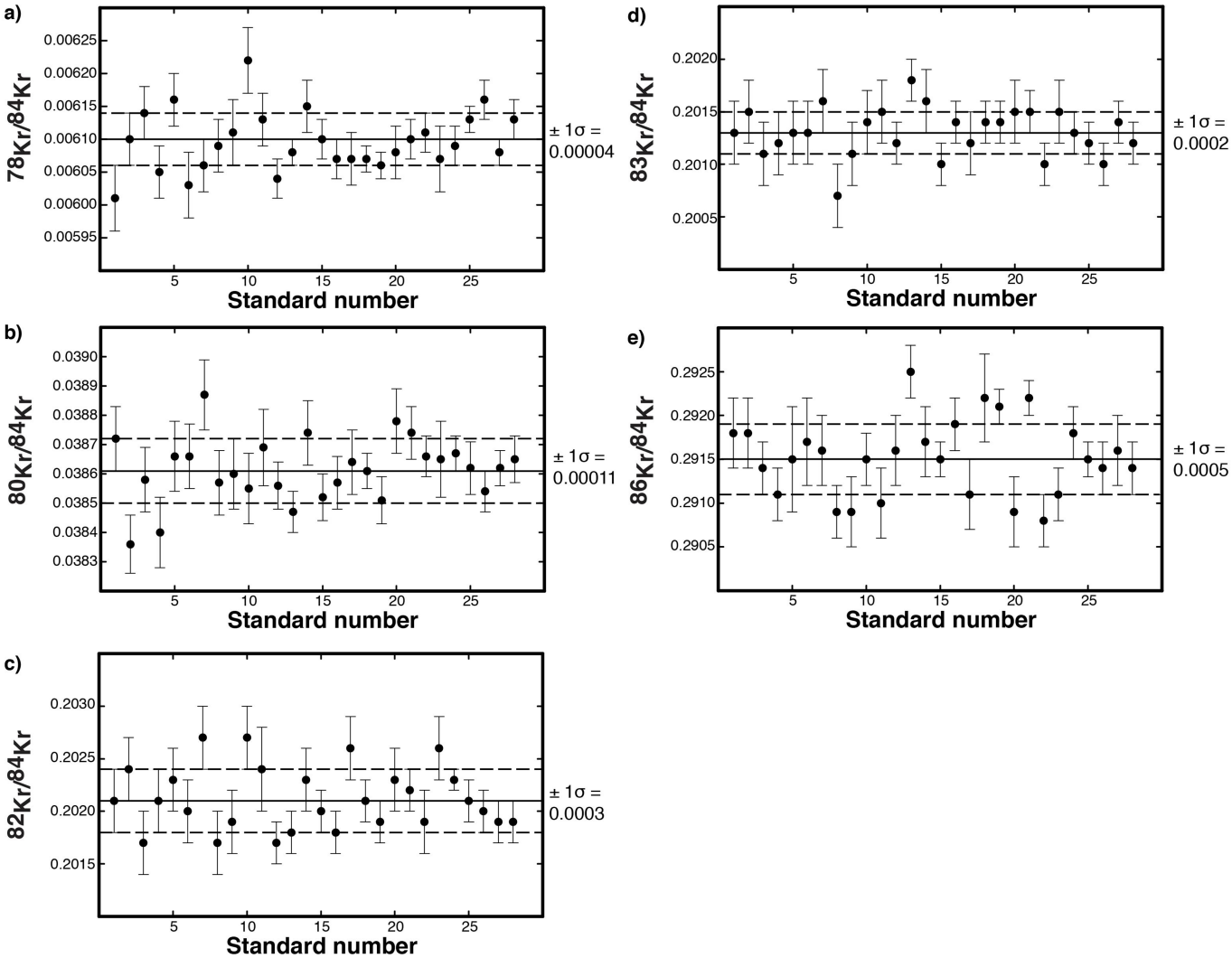

Extended Data Fig. 4 | Reproducibility of the air standard for krypton isotopic ratios. a, $^{78}Kr/^{84}Kr$. **b**, $^{80}Kr/^{84}Kr$. **c**, $^{82}Kr/^{84}Kr$. **d**, $^{83}Kr/^{84}Kr$. **e**, $^{86}Kr/^{84}Kr$. This set of standards was measured over 13 days and include three sizes of air standard, ranging from 7.52×10^{-12} cc to 2.37×10^{-11} cc of ^{84}Kr. For the samples, only one size of the air standard was used (^{84}Kr of 2.37×10^{-11} cc), measurements of this air standard size show an even better reproducibility (typically of 2‰ for $^{78}Kr/^{84}Kr$, of 2.5‰ for $^{80}Kr/^{84}Kr$, of 1‰ for $^{82}Kr/^{84}Kr$, of 1.5‰ for $^{83}Kr/^{84}Kr$ and of 1‰ for $^{86}Kr/^{84}Kr$).

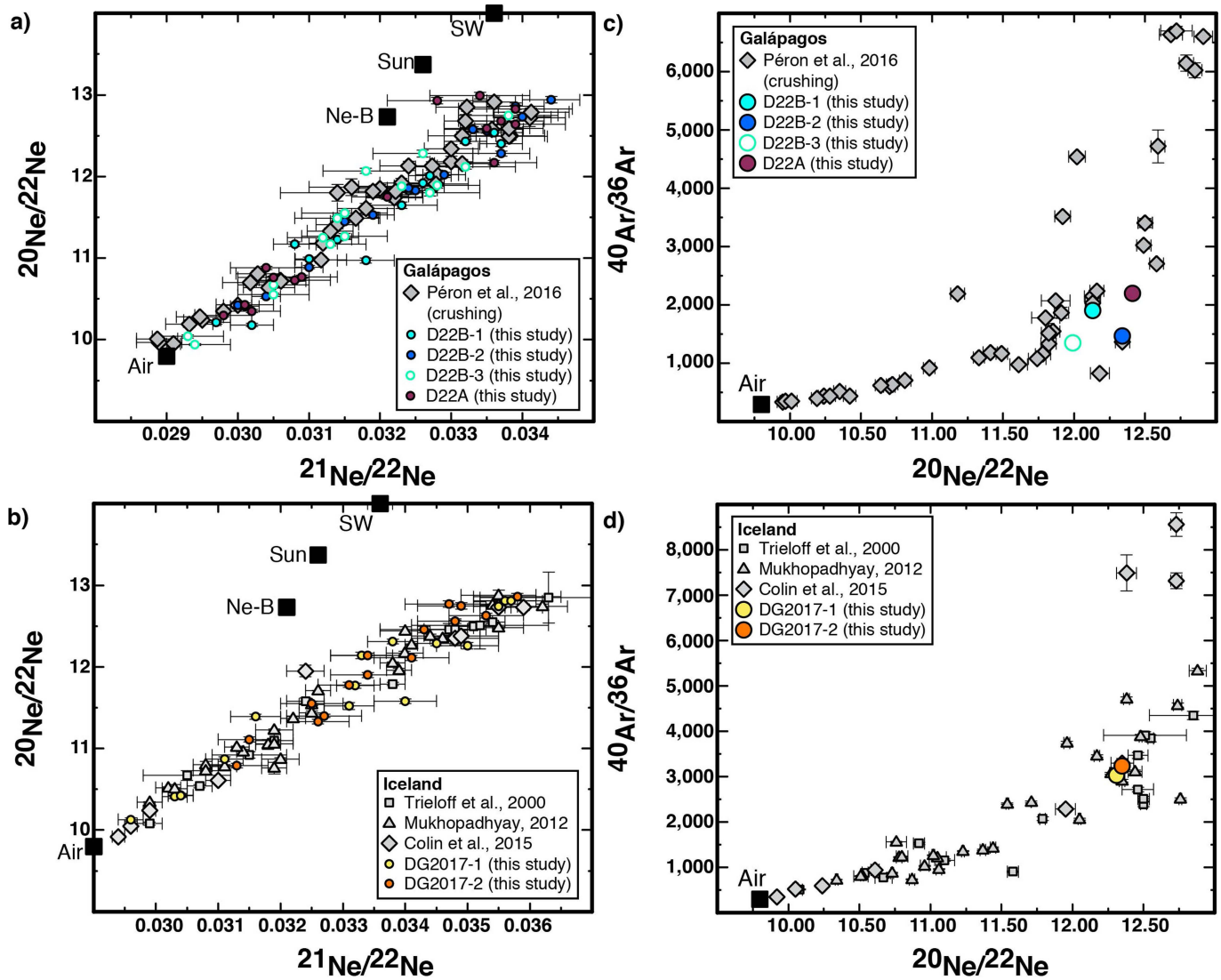

Extended Data Fig. 5 | Three-neon isotope plot for the step-crushing analyses and argon–neon isotope plot for the accumulated gas. a, Neon isotopic ratios for samples D22B-1, D22B-2, D22B-3 and D22A (Galápagos), compared with literature data[11]. **b**, Neon isotopic ratios for samples DG2017-1 and DG2017-2 (Iceland), compared with literature data[14,15,54]. Supplementary Table 2 indicates for which step heavy noble gases were accumulated. Neon-B[4], Sun[83], solar wind[84]. **c**, $^{40}Ar/^{36}Ar$ versus $^{20}Ne/^{22}Ne$ for samples D22B-1, D22B-2, D22B-3 and D22A (Galápagos), compared with literature data[11]. **d**, $^{40}Ar/^{36}Ar$ versus $^{20}Ne/^{22}Ne$ for samples DG2017-1 and DG2017-2 (Iceland) compared with literature data[14,15,54]. The $^{20}Ne/^{22}Ne$ ratios for samples D22B-1, D22B-2, D22B-3, D22A, DG2017-1 and DG2017-2 are the average ratios of the accumulated steps, refer to Supplementary Table 2. The measured $^{40}Ar/^{36}Ar$ ratios as well as the average $^{20}Ne/^{22}Ne$ ratios are consistent with previous measurements for these same samples.

Extended Data Table 1 | Krypton isotopic compositions of samples AHA-NEMO2-D22A and AHA-NEMO2-D22B (hereafter D22A and D22B, Fernandina, Galápagos, respectively) and DG2017 (Midfell, Iceland)

Sample	^{84}Kr ($\times 10^{-11}$ cm^{3}STP)	^{78}Kr/^{84}Kr	^{80}Kr/^{84}Kr	^{82}Kr/^{84}Kr	^{83}Kr/^{84}Kr	^{86}Kr/^{84}Kr
D22B-1	1.61	0.00602	0.03941	0.2021	0.2016	0.3053
+/-	0.02	0.00003	0.00017	0.0005	0.0004	0.0006
D22B-2	3.10	0.00603	0.03941	0.2015	0.2017	0.3065
+/-	0.05	0.00003	0.00020	0.0004	0.0004	0.0004
D22B-3	2.30	0.00601	0.03894	0.2006	0.2006	0.3070
+/-	0.04	0.00004	0.00017	0.0005	0.0003	0.0007
D22A	1.22	0.00604	0.03956	0.2023	0.2015	0.3053
+/-	0.04	0.00005	0.00019	0.0006	0.0004	0.0007
D22 (average)		**0.00603**	**0.03932**	**0.2016**	**0.2012**	**0.3061**
+/-		**0.00002**	**0.00009**	**0.0002**	**0.0002**	**0.0003**
DG2017-1	2.19	0.00605	0.03949	0.2024	0.2016	0.3059
+/-	0.04	0.00003	0.00012	0.0003	0.0003	0.0004
DG2017-2	2.42	0.00601	0.03947	0.2019	0.2013	0.3056
+/-	0.08	0.00004	0.00021	0.0006	0.0004	0.0007
DG2017 (average)		**0.00604**	**0.03948**	**0.2023**	**0.2015**	**0.3058**
+/-		**0.00002**	**0.00011**	**0.0002**	**0.0003**	**0.0004**
Air		0.00609	0.03960	0.2022	0.2014	0.3052
AVCC		0.00595	0.03928	0.2008	0.2007	0.3092
+/-		0.00002	0.00006	0.0003	0.0002	0.0002
Phase Q		0.00603	0.03937	0.2018	0.2018	0.3095
+/-		0.00003	0.00007	0.0002	0.0002	0.0005
Solar Wind		0.00642	0.04120	0.2054	0.2034	0.3012
+/-		0.00005	0.00020	0.0002	0.0002	0.0004

The weighted averages of the four Galápagos and the two Iceland measurements are reported. Compositions of air[73], AVCC, Phase Q[25] and solar wind[24] are indicated for comparison. ^{84}Kr is reported as the total amount measured in cm^3 STP and not divided by the sample mass. Sample D22B-1 was 4.04599 g, sample D22B-2 was 4.09500 g, sample D22B-3 was 3.0052 g, sample D22A was 4.1554 g, sample DG2017-1 was 4.5371 g and sample DG2017-2 was 4.7092 g. Refer to text and Extended Data Table 3 for the calculation of the AVCC end-member. Uncertainties are 1σ.

Extended Data Table 2 | Xenon abundances and isotopic ratios measured with the accumulation protocol for the Galápagos (AHA-NEMO2-D22A and AHA-NEMO2-D22B) and Iceland (DG2017) samples

Sample	^{130}Xe x10^{-13} cm^{3}STP	^{124}Xe/^{130}Xe	^{126}Xe/^{130}Xe	^{128}Xe/^{130}Xe	^{129}Xe/^{130}Xe	^{131}Xe/^{130}Xe	^{132}Xe/^{130}Xe	^{134}Xe/^{130}Xe	^{136}Xe/^{130}Xe
D22B-1	1.57	0.0236	0.0215	0.4723	6.66	5.23	6.65	2.59	2.23
+/-	0.04	0.0006	0.0006	0.0033	0.03	0.02	0.03	0.01	0.01
D22B-2	3.05	0.0231	0.0212	0.4768	6.61	5.23	6.63	2.59	2.21
+/-	0.07	0.0006	0.0005	0.0030	0.03	0.04	0.04	0.03	0.01
D22B-3	1.97	0.0234	0.0223	0.4740	6.63	5.23	6.65	2.60	2.23
+/-	0.04	0.0007	0.0007	0.0035	0.03	0.02	0.03	0.01	0.01
D22A	1.13	0.0227	0.0218	0.4695	6.70	5.20	6.63	2.61	2.22
+/-	0.06	0.0007	0.0006	0.0034	0.05	0.04	0.04	0.02	0.02
D22 (average)		**0.0232**	**0.0216**	**0.4734**	**6.64**	**5.22**	**6.64**	**2.60**	**2.22**
+/-		**0.0003**	**0.0003**	**0.0016**	**0.02**	**0.01**	**0.02**	**0.01**	**0.01**
DG2017-1	2.37	0.0236	0.0223	0.4715	6.74	5.23	6.64	2.62	2.25
+/-	0.04	0.0004	0.0005	0.0024	0.04	0.03	0.03	0.02	0.01
DG2017-2	2.31	0.0241	0.0224	0.4754	6.79	5.22	6.66	2.62	2.26
+/-	0.07	0.0008	0.0008	0.0036	0.03	0.03	0.03	0.01	0.01
DG2017 (average)		**0.0237**	**0.0223**	**0.4727**	**6.78**	**5.22**	**6.65**	**2.62**	**2.25**
+/-		**0.0004**	**0.0004**	**0.0020**	**0.03**	**0.02**	**0.02**	**0.01**	**0.01**
Air		0.0234	0.0218	0.4710	6.50	5.21	6.61	2.56	2.18

Uncertainties are 1σ.

Extended Data Table 3 | Compilation of carbonaceous, ordinary and enstatite chondrites krypton isotopic data[67–70,80–82]

Meteorites	Class	$^{78}Kr/^{84}Kr$	σ	$^{80}Kr/^{84}Kr$	σ	$^{82}Kr/^{84}Kr$	σ	$^{83}Kr/^{84}Kr$	σ	$^{86}Kr/^{84}Kr$	σ
Carbonaceous chondrites (CC)											
Murray[68]	CM2	0.00594	0.00009	0.03938	0.00053	0.2006	0.0020	0.2009	0.0018	0.3093	0.0019
Murray[70]	CM2					0.1988	0.0016	0.1994	0.0014	0.3068	0.0024
Cold Bokkeveld[67]	CM2	0.00597	0.00004	0.03915	0.00030	0.2013	0.0008	0.2014	0.0009	0.3092	0.0008
Orgeuil[70]	CI1					0.1998	0.0012	0.2001	0.0012	0.3091	0.0015
Orgeuil[67]	CI1	0.00588	0.00008	0.03922	0.00042	0.2011	0.0016	0.2011	0.0016	0.3090	0.0015
Lance[68]	CO3.5	0.00591	0.00011	0.03948	0.00059	0.2006	0.0026	0.2013	0.0024	0.3093	0.0029
Lance[67]	CO3.5	0.00600	0.00008	0.03958	0.00046	0.2017	0.0015	0.2013	0.0014	0.3099	0.0012
Leoville[69]	CV3			0.03824	0.00030	0.2009	0.0012	0.2005	0.0010	0.3090	0.0010
AVCC		**0.00595**	**0.00002**	**0.03928**	**0.00006**	**0.2008**	**0.0003**	**0.2007**	**0.0002**	**0.3092**	**0.0002**
Ordinary chondrites (OC)											
Dimmitt[80]	H3.7	0.00583	0.00023					0.2019	0.0040	0.3089	0.0038
Mezö Madaras[80]	L3.5	0.00591	0.00017					0.2014	0.0027	0.3112	0.0029
Parnallee[80]	LL3	0.00595	0.00010					0.2021	0.0016	0.3104	0.0029
Tieschitz 1[80]	H3.6	0.00599	0.00017					0.2012	0.0036	0.3105	0.0029
Tieschitz 4[80]	H3.6	0.00605	0.00006					0.2013	0.0013	0.3088	0.0014
Average OC		**0.00601**	**0.00003**					**0.2016**	**0.0002**	**0.3097**	**0.0005**
Enstatite chondrites (EC)											
ALH84206[81]	EH3							0.2020	0.0010	0.3070	0.0010
ALH 77295[82]	EH3							0.2026	0.0004	0.3124	0.0005
Sahara 97096[82]	EH3							0.2020	0.0005	0.3102	0.0006
Y-691[82]	EH3							0.2034	0.0004	0.3142	0.0004
Y-792959[82]	EH3							0.2014	0.0004	0.3113	0.0005
Y-793161[82]	EH3							0.2017	0.0004	0.3094	0.0006
Average EC								**0.2022**	**0.0003**	**0.3118**	**0.0008**

Data are normalized to the atmospheric composition used in this study[73]. The Leoville data[69], ordinary[80] and enstatite chondrites[81,82] data were corrected for cosmogenic component (refer to Methods for details).

Extended Data Table 4 | Argon abundances and isotopic ratios measured with the accumulation protocol for the Galápagos (AHA-NEMO2-D22A and AHA-NEMO2-D22B) and Iceland (DG2017) samples

Sample	^{36}Ar	σ	$^{38}Ar/^{36}Ar$	σ	$^{40}Ar/^{36}Ar$	σ
	$x10^{-10}$ cm^3STP					
AHA-NEMO2-D22B-1	5.75	0.10	0.1879	0.0003	1902.6	1.0
AHA-NEMO2-D22B-2	9.73	0.20	0.1885	0.0003	1464.2	1.0
AHA-NEMO2-D22B-3	8.26	0.02	0.1884	0.0003	1347.2	1.0
AHA-NEMO2-D22A	4.25	0.03	0.1879	0.0003	2195.4	1.0
DG2017-1	5.01	0.02	0.1880	0.0004	3025.2	1.0
DG2017-2	7.95	0.05	0.1889	0.0002	3228.8	1.0
Air			0.1880		295.5	

As mentioned in the text, the values for argon cannot be used as representative of the source compositions. Uncertainties are 1σ.

Extended Data Table 5 | Results of the accumulation tests with air standard aliquots of 7.52×10^{-12} cc of ^{84}Kr

	$^{78}Kr/^{84}Kr$	s	$^{80}Kr/^{84}Kr$	s	$^{82}Kr/^{84}Kr$	s	$^{83}Kr/^{84}Kr$	s	$^{86}Kr/^{84}Kr$	s
Test 1	0.00606	0.00003	0.04010	0.00007	0.2030	0.0002	0.2020	0.0002	0.2900	0.0003
Test 2	0.00611	0.00003	0.04006	0.00007	0.2034	0.0002	0.2021	0.0002	0.2907	0.0002
Test 3	0.00607	0.00003	0.04004	0.00008	0.2033	0.0002	0.2022	0.0002	0.2903	0.0002
Average	0.00608	0.00003	0.04007	0.00003	0.2032	0.0002	0.2021	0.0001	0.2903	0.0004
Average 7.52×10^{-12} cc of ^{84}Kr (n = 16)	0.00609	0.00003	0.04021	0.00010	0.2036	0.0004	0.2022	0.0003	0.2902	0.0003
Measurements of air standard of 2.37×10^{-11} cc of ^{84}Kr										
STD 1	0.00611	0.00002	0.04023	0.00009	0.2033	0.0002	0.2025	0.0002	0.2903	0.0002
STD 2	0.00608	0.00002	0.04034	0.00006	0.2037	0.0002	0.2024	0.0002	0.2903	0.0002
STD 3	0.00612	0.00003	0.04034	0.00006	0.2036	0.0003	0.2023	0.0003	0.2901	0.0002
STD 4	0.00606	0.00002	0.04011	0.00007	0.2031	0.0002	0.2023	0.0002	0.2902	0.0002
STD 5	0.00611	0.00003	0.04019	0.00008	0.2030	0.0002	0.2024	0.0002	0.2905	0.0003
Average (n = 5)	0.00610	0.00003	0.04024	0.00010	0.2033	0.0003	0.2024	0.0001	0.2903	0.0001

Each test consists of the accumulation of three air standard aliquots of 7.52×10^{-12} cc of ^{84}Kr. The test results are compared with measurements of air aliquots of 7.52×10^{-12} cc (average of $n = 16$ analyses) and of 2.37×10^{-11} cc (average of $n = 5$ analyses) of ^{84}Kr. The measured Kr isotopic ratios from the accumulation tests are similar to the ones for air standard aliquots of 7.52×10^{-12} cc and of 2.37×10^{-11} cc of ^{84}Kr.